Kinetics of Oxide Film Growth on Metal Crystals: Electronic and Ionic Diffusion in Large Surface-Charge and Space-Charge Fields

A. T. FROMHOLD, JR., AND EARL L. COOK*
Department of Physics, Auburn University, Auburn, Alabama 36830
(Received 3 June 1968)

The coupled-currents approach is utilized to study oxidation kinetics for the case of electron and ion transport by field-modified diffusion. The expression developed for the particle current J for a given species is $J=(\nu/S_N)\exp(-W/k_BT)[n_0-n_N\exp(ZeV_N/k_BT)]$, with $S_N=\sum_{k=1}^{N}\exp[Ze(V_{k-1}+V_k)/2k_BT]$, where ν, W, n_0, n_N, and Z are, respectively, the attempt frequency, activation barrier, areal density at the metal-oxide interface, areal density at the oxide-oxygen interface, and charge per particle in units of e for the diffusing defect species in question; k_B, T, and e denote the Boltzmann constant, the temperature, and the electronic-charge magnitude. The macroscopic electrostatic potential at the position of the potential minimum following the kth potential maximum due to the ordinary lattice periodicity is denoted by V_k. In the low-space-charge high-field limit for equal magnitudes of Z for the oppositely charged diffusing species, the electrostatic potential developed across the film is a constant, and the resulting kinetics have the Mott-Cabrera form. The time t as a function of film thickness L is given by a series of second-order exponential integrals E_2 with successively increasing values of the argument:

$$t/\tau=2\frac{L}{L_{\text{crit}}}\sum_{m=0}^{\infty}E_2\left((2m+1)\frac{L_{\text{crit}}}{L}\right),$$

where τ and L_{crit} are determined by the transport parameters for the system in question. This expression reduces to the previously derived homogeneous-field parabolic growth law $L^2=2L_{\text{crit}}^2t/\tau$ whenever nonlinear effects become inappreciable. Space charge can retard, enhance, or provide no modification of the growth rate, depending on the potential developed across the film and the sign of the space charge relative to the rate-limiting species. For nonzero potentials with the sign of the space charge opposite to that of the rate-limiting species, the growth rate is found to be enhanced; for nonzero potentials with the sign of the space charge the same as that of the rate-limiting species, the growth rate is found to be retarded.

I. INTRODUCTION

THE effect of space charge on electronic and ionic transport in semiconducting and insulator-type solids is an important physical problem to which considerable attention has been given in the literature.[1–5] The space-charge modifications of the values of such transport currents introduce changes in the kinetics of growth of dielectric and semiconducting contact layers on metals, since the rate of growth of such layers is determined by the rate of charged particle transport through the layer.[6] Some consideration has already been given to the possible modification of the oxidation kinetics whenever space charge is important.[7–10] Because of the complexity of the system of coupled nonlinear diffusion equations, however, the analytical approaches to date have been approximate. Exact numerical computations are a necessity in order to verify the predictions of previous treatments of an approximate nature and to provide a basis for further analytical development.

The present work consists of exact numerical solutions for oxidation kinetics based on electronic and ionic diffusion currents with space charge. The computations represent solutions for the early growth stage in which space charge initially becomes an important factor in the kinetics; the numerical scheme utilized for the computations did not allow the computations to be carried into the thick-film limit where total neutralization of the space charge has been considered.[6] The method utilized for obtaining the kinetics is that of "coupled currents" which has been utilized previously to examine models of thin-film oxidation kinetics based on electron tunneling[11] and thermal electron emission.[12,13] The present development is applicable in the growth region in which electron tunneling is negligible and the scattering of thermally emitted electrons in the oxide conduction band is sufficient to establish an electron concentration gradient. There is evidence[14] that this thickness may be of the order of 25 Å. The present equations include nonlinear diffusion effects due to large

* Present address: Central Research Laboratories, 3M Company, St. Paul, Minnesota. This research was performed at Auburn University in partial fulfillment of the requirements for the Ph.D. degree.

[1] H. Y. Fan, Phys. Rev. **74**, 1505 (1948).
[2] W. van Roosbroeck, Phys. Rev. **123**, 474 (1961).
[3] G. T. Wright, Solid-State Electron. **2**, 165 (1961).
[4] J. Ross Macdonald, Solid-State Electron. **5**, 11 (1962).
[5] M. A. Lampert, Rept. Progr. Phys. **27**, 329 (1964).
[6] C. Wagner, Z. Physik. Chem. (Frankfurt) **B21**, 25 (1933).
[7] K. Hauffe, *Oxidation of Metals* (Plenum Press, Inc., New York, 1965), p. 109.
[8] A. T. Fromhold, Jr., J. Phys. Chem. Solids **25**, 1129 (1964).
[9] A. T. Fromhold, Jr., J. Chem. Phys. **40**, 3335 (1964).
[10] A. T. Fromhold, Jr., and E. R. Graf, J. Chem. Phys. **44**, 1628 (1966).
[11] A. T. Fromhold, Jr., and E. L. Cook, Phys. Rev. **158**, 600 (1967).
[12] A. T. Fromhold, Jr., and E. L. Cook, Phys. Rev. **163**, 650 (1967).
[13] A. T. Fromhold, Jr., and E. L. Cook, Phys. Rev. Letters **17**, 1212 (1966).
[14] R. C. Chapman, J. Appl. Phys. **35**, 2832 (1964).
[15] N. F. Mott, Trans. Faraday Soc. **43**, 431 (1947).

electric fields in discrete lattices as considered by Mott[15] and by Cabrera and Mott.[16]

The basic equations are formulated in Sec. II. Oxidation kinetics in the zero space-charge limit are considered in Sec. III. Numerical computations illustrating space-charge modifications in the kinetics and concentration profiles are illustrated in Sec. IV. Conclusions are summarized in Sec. V.

II. FORMULATION OF EQUATIONS

The discrete model previously developed[17] for diffusion currents is utilized without making the simplifying homogeneous field approximation. Thus the space-charge contribution to the electric field, as given by Poisson's equation considering two or more oppositely charged diffusing species, is included in the present development of equations for diffusion currents.

Discrete Lattice

The lattice is considered to consist of N potential barriers of equal height $W^{(s)}$ for the sth diffusing species (e.g., cation or anion vacancies, cation or anion interstitials, electrons, or electron holes). A diagram illustrating the barriers and appropriate notation is given in Fig. 1 of Ref. 17. The factor of the discreteness of the lattice must definitely be included in order to obtain a valid microscopic derivation of the current for large electric fields.[17] The one-dimensional geometry utilized is applicable for the case of the growth of uniform oxides on flat metal surfaces, since the diffusion currents for growth of the oxide are then directed normal to the metal-oxide interface. The potential maxima are considered to be located at positions x_k $(k=1, 2, \cdots, N)$, where $x_k=(2k-1)a$, with $2a$ representing the distance between the potential barriers along the direction of the current. The potential minima are located at the positions $x=0$ and $x_k+a=2ka$ $(k=1, 2, \cdots, N)$. The total thickness $L(t)$ of the oxide is thus $x_N+a=2Na$.

The potential minimum located at $(x_k+a)=2ka$ for arbitrary k is given the index k. Thus potential minima occur at $x=0$, $2a$, $4a$, $\cdots$, $2Na$ and potential maxima occur at $x=a$, $3a$, $5a$, $\cdots$, $(2N-1)a$.

The areal density (particles/cm^2 in a plane normal to the direction of the current) of a given type s of diffusing particles (interstitials, vacancies, electrons, or electron holes) at the kth potential minimum is given by $n_k^{(s)}$. It should be emphasized that $n^{(s)}$ represents the defect concentration (i.e., the deviation from the value appropriate for a perfect lattice) of the sth species rather than the stoichiometric concentration of the sth species appropriate for a perfect lattice, since the defect concentrations are responsible for the space charge, and defect gradients provide the driving force for diffusion currents. The bulk defect concentration equivalent to the $n_k^{(s)}$ at the point in question is given by $n_k^{(s)}/2a$.

The electrostatic potential at the kth potential minimum (for arbitrary k) is denoted by V_k. The relationships between the electrostatic potentials, electric fields, and areal densities of the diffusing species can now be stated in terms of the present notation in a manner consistent with Poisson's equation[18] of electrostatics.

Electric Fields

Define the quantities E_k $(k=1, 2, \cdots, N)$ as the electric field at the position of the potential maxima, i.e., $E_k=E(x_k)$. The electric field differs from potential maximum to potential maximum because of the areal densities of charged diffusing species in the intervening potential minimum. Thus for r diffusing species,

$$E_k=E_{k-1}+(4\pi/\epsilon)[q^{(1)}n_{k-1}^{(1)}+q^{(2)}n_{k-1}^{(2)}+\cdots+q^{(r)}n_{k-1}^{(r)}] \quad (k=1, 2, \cdots, N), \quad (2.1)$$

where $q^{(s)}$ is the actual electric charge (i.e., the deviation from a charge neutral lattice resulting in a contribution to the macroscopic space-charge distribution) associated with each particle of the sth diffusing defect species. With E_k defined in this manner, E_0 is the surface-charge electric field at the metal-oxide interface excluding the areal densities of charged particles at the potential minimum with index 0 (i.e., at $x=0$). The source of E_0 is considered to be the net charge on the metal at $x=0$, as distinguished from the charged defects in the zeroth potential minimum in the oxide.

Utilizing the notation of finite differences,[19] where the first difference of an arbitrary function f is defined by

$$\Delta f_k \equiv f_{k+1}-f_k, \quad (2.2)$$

the first difference of the electric field given by (2.1) is thus

$$\Delta E_j=(4\pi/\epsilon)\sigma_j \quad (j=0, 1, 2, \cdots, N-1), \quad (2.3)$$

where σ_j is the net charge associated with the jth potential minimum due to all diffusing species,

$$\sigma_j=\sum_{s=1}^{r} q^{(s)}n_j^{(s)} \quad (j=0, 1, 2, \cdots, N). \quad (2.4)$$

That is, σ_j is the total areal charge density at the position of the jth potential minimum. An additional quantity of charge necessary for charge neutrality of the metal-oxide system as a whole is considered to reside in surface states provided by adsorbed oxygen at the oxide-oxygen interface. A summation of (2.3) from $j=0$

[16] N. Cabrera and N. F. Mott, Rept. Progr. Phys. **12**, 163 (1949).

[17] A. T. Fromhold, Jr., and E. L. Cook, J. Appl. Phys. **38**, 1546 (1967).

[18] J. D. Jackson, *Classical Electrodynamics* (John Wiley & Sons, Inc., New York, 1962), p. 12.

[19] C. Jordan, *Calculus of Finite Differences* (Chelsea Publishing Co., New York, 1965), p. 2.

to $j=k-1$ yields

$$\sum_{j=0}^{k-1}\Delta E_j=E_k-E_0=\frac{4\pi}{\epsilon}\sum_{j=0}^{k-1}\sigma_j \quad (k=1, 2, \cdots, N). \quad (2.5)$$

Electrostatic Potentials

Since the charged particles are considered to be located predominantly in the potential minima, the macroscopic electric field E_k $(k=1, 2, \cdots, N)$ can be considered to be essentially uniform in value over regions $x_k-a\leqq x<x_k+a$ of the order of a lattice parameter. This statement is consistent with expression (2.1) for the field. The change in electrostatic potential between adjacent potential minima is then given by

$$\Delta V_{k-1}\equiv V_k-V_{k-1}=-2aE_k \quad (k=1, 2, \cdots, N). \quad (2.6)$$

The reasonableness of this equation becomes apparent when it is recalled that E_k is defined at the kth potential maximum whereas V_{k-1} and V_k are defined, respectively, at the potential minima preceding and following the kth potential barrier. Taking the second difference of (2.6) and substituting (2.3) then yields

$$\Delta^2V_{k-1}\equiv\Delta(\Delta V_{k-1})=-2a\Delta E_k=-(8\pi a/\epsilon)\sigma_k \quad (k=1, 2, \cdots, N). \quad (2.7)$$

This is the discrete analog of Poisson's equation.

On the other hand, substitution of (2.5) into (2.6) and summation from $k=1$ to $k=m$ yields

$$\sum_{k=1}^{m}\Delta V_{k-1}=V_m-V_0=-2a\sum_{k=1}^{m}E_k=-2amE_0-\frac{8\pi a}{\epsilon}\sum_{k=1}^{m}\sum_{j=0}^{k-1}\sigma_j \quad (m=1, 2, \cdots, N). \quad (2.8)$$

The double sum can be rearranged and written as a single sum, so that (2.8) becomes

$$V_m-V_0=-2amE_0-\frac{8\pi a}{\epsilon}\sum_{j=0}^{m-1}(m-j)\sigma_j. \quad (2.9)$$

The surface-charge field E_0 at the metal interface can be related to the total difference of potential (V_N-V_0) across the oxide by letting $m=N$ in (2.9):

$$E_0=(-2aN)^{-1}\left[(V_N-V_0)+\frac{8\pi a}{\epsilon}\sum_{j=0}^{N-1}(N-j)\sigma_j\right]. \quad (2.10)$$

It is illuminating to recall that $2aN$ is simply the total thickness $L(t)$ of the oxide. Equation (2.10) shows that in principle it is immaterial which of the two parameters (E_0, V_N-V_0) is chosen for discussing a calculation in which neither of the two is held fixed at the outset, since they are related through Eq. (2.10). It has been found in practice that V_N does not vary appreciably with N for the present work, a result of great importance in application of previous perturbation and averaging techniques,[8–10] so that it is conceptually an easier parameter to consider for this set of numerical calculations. Substitution of (2.10) into (2.9) thus yields the following:

$$V_m-V_0=(m/N)\left[(V_N-V_0)+\frac{8\pi a}{\epsilon}\sum_{j=0}^{N-1}(N-j)\sigma_j\right]-\frac{8\pi a}{\epsilon}\sum_{j=0}^{m-1}(m-j)\sigma_j=\frac{m}{N}(V_N-V_0)+\frac{8\pi a}{\epsilon}\left[\sum_{j=0}^{m-1}j\left(1-\frac{m}{N}\right)\sigma_j+\sum_{j=m}^{N-1}m\left(1-\frac{j}{N}\right)\sigma_j\right] \quad (m=1, 2, \cdots, N-1). \quad (2.11)$$

The zero of potential is arbitrary, as usual, since only differences of potential occur in the above equations. It is therefore convenient to choose $V_0=0$. This is done throughout the remainder of the equations; this is the convention used throughout in our numerical computations.

Particle Currents

The equation for the particle currents $J_k^{(s)}$ of the sth species over the kth potential barrier can now be stated. Each current is the difference between the forward current due to the particles with areal density $n_{k-1}^{(s)}$ attempting the kth barrier with frequency $\nu^{(s)}$, and the reverse current due to the particles with areal density $n_k^{(s)}$ attempting the same barrier with the same frequency. The barrier height $W_f^{(s)}$ for the forward direction is modified to $W^{(s)}-Z^{(s)}eE_ka$ by the presence of the electric field E_k, and the corresponding value $W_r^{(s)}$ for the reverse direction is $W^{(s)}+Z^{(s)}eE_ka$. The parameter e is the magnitude of the electronic charge and $Z^{(s)}e$ is the *effective* charge[17] (magnitude and sign) of the diffusing species for migration in the polarizable and partially covalent medium in which the macroscopic electric field is E_k. The quantity $Z^{(s)}e$ has recently been stated by Dignam[20] and previously by Lidiard[21] to be equal to the space-charge contribution per particle of the sth species; an alternate justification is given in Appendix A. Even though the quantities $q^{(s)}$ and $Z^{(s)}e$ may have the same average numerical value, and have always been chosen numerically equal in our calculations, we prefer to retain the different notations for these quantities in our equations to emphasize the two roles (i.e., space-charge contribution to the macroscopic electric field and force per particle located in the field surrounded by the polarized lattice) which the charge on each particle plays in the diffusion phenomenon.

[20] M. J. Dignam, J. Electrochem. Soc. **112**, 722 (1965); J. Phys. Chem. Solids **29**, 249 (1968). (The later represents a reversal in opinion over the former as regards the question of internal electric field modifications of the diffusion current.)

[21] A. B. Lidiard, in *Handbuch der Physik*, edited by S. Flügge (Springer-Verlag, Berlin, 1957), Vol. 20, p. 324.

Assuming Boltzmann statistics for the probability that the diffusing particle has a given energy as a result of thermal vibrations of the lattice, the relation for the particle current [Eq. (2.5) of Ref. 17] follows immediately:

$$J_k^{(s)}=\nu^{(s)}\exp(-W^{(s)}/k_BT)[n_{k-1}^{(s)}\exp(Z^{(s)}eE_ka/k_BT)-n_k^{(s)}\exp(-Z^{(s)}eE_ka/k_BT)]$$
$$(k=1,2,\cdots,N;\ s=1,2,\cdots,r), \quad (2.12)$$

where k_B is the Boltzmann constant and T is the absolute temperature. The currents are thus defined at the positions x_k of the potential barrier maxima.

Equation (2.12) neglects second-order effects of the electric field. These effects, which are due to a relative shift in the potential maxima with respect to the potential minima that is asymmetrical in the forward and reverse directions, were first discussed by Dignam.[22] An independent treatment is given in Appendix II of Ref. 17. In view of the simplicity of the model utilized for the diffusion process in developing Eq. (2.12), and the fact that only "built-in" potentials are present in thermal oxidation (in contrast to the possibility of much larger "applied" potentials in the anodic oxidation[23] case), it was decided to ignore second-order effects entirely in the present development. This is in accordance with the treatment of ionic diffusion in our previous developments[11–13] of oxidation kinetics for the cases of electron tunneling and thermal electron emission.

Steady State

The consideration of the diffusion currents is now restricted to the limit of the steady state in the presence of the surface-charge field and the space-charge distribution appropriate for the given thickness and the given values of the physical parameters. The steady state is the nonzero particle current situation obtained in the theoretical limit in which the two boundaries of the oxide film are not moving relative to each other, and following a time lapse sufficient for all transients to disappear from the system. In this limit, the particle currents are uniform (divergenceless) throughout the lattice, having sources and sinks only at the metal-oxide interface and at the oxide-oxygen interface. Exact numerical computations[24] using the non-steady-state continuum equation for simple diffusion have shown the steady-state approximation to be well justified for growth rates (and corresponding particle currents) which are physically realistic for thermal oxidation. The mathematical statement of the steady-state approximation for the sth species in the case of a discrete lattice is

$$\partial n_k^{(s)}/\partial t=J_k^{(s)}-J_{k+1}^{(s)}\equiv-\Delta J_k^{(s)}\simeq 0$$
$$(k=1,2,\cdots,N-1). \quad (2.13)$$

Thus each of the variables $J_k^{(s)}$ can be replaced by the single parameter $J^{(s)}$,

$$J_k^{(s)}=J^{(s)} \quad (k=1,2,\cdots,N;\ s=1,2,\cdots,r), \quad (2.14)$$

where $J^{(s)}$ still remains to be determined.

Partial Summation of Difference Equations

A partial summation of the set of equations (2.12) for the currents and the areal concentrations can be effected in the limit of the steady state. This summation considerably simplifies the process of obtaining practical numerical solutions; it also renders the problem amenable to an analytical solution for certain cases.

Substituting Eq. (2.14) for the steady state and utilizing (2.6) to replace the electric fields by the corresponding first differences of the potential, Eq. (2.12) becomes

$$J^{(s)}=\nu^{(s)}\exp(-W^{(s)}/k_BT)\times[n_{k-1}^{(s)}\exp(-Z^{(s)}e\Delta V_{k-1}/2k_BT)-n_k^{(s)}\exp(Z^{(s)}e\Delta V_{k-1}/2k_BT)]$$
$$(k=1,2,\cdots,N;\ s=1,2,\cdots,r). \quad (2.15)$$

Let $V_0=0$ as mentioned previously, and for convenience introduce the following quantities:

$$\alpha_k^{(s)}\equiv\exp(-Z^{(s)}e\Delta V_{k-1}/k_BT), \quad (2.16)$$

$$F_k^{(s)}\equiv\exp(-Z^{(s)}eV_k/k_BT), \quad (2.17)$$

$$\zeta^{(s)}=(J^{(s)}/\nu^{(s)})\exp(W^{(s)}/k_BT). \quad (2.18)$$

Substitution of (2.16) and (2.18) into (2.15) and multiplication by $(\alpha_k^{(s)})^{1/2}/F_k^{(s)}$ transforms (2.15) into the form

$$\zeta^{(s)}(\alpha_k^{(s)})^{1/2}/F_k^{(s)}=(n_{k-1}^{(s)}\alpha_k^{(s)}/F_k^{(s)})-(n_k^{(s)}/F_k^{(s)})=-\Delta(n_{k-1}^{(s)}/F_{k-1}^{(s)}), \quad (2.19)$$

where the definition (2.2) has been utilized. A summation of (2.19) from $k=1$ to $k=j$ yields

$$\zeta^{(s)}S_j^{(s)}=n_0^{(s)}-(n_j^{(s)}/F_j^{(s)}), \quad (2.20)$$

where

$$S_j^{(s)}\equiv\sum_{k=1}^{j}\frac{(\alpha_k^{(s)})^{1/2}}{F_k^{(s)}}=\sum_{k=1}^{j}\exp\left(\frac{Z^{(s)}e(V_{k-1}+V_k)}{2k_BT}\right). \quad (2.21)$$

Equation (2.20) for the case $j=N$ yields an evaluation of $\zeta^{(s)}$, and therefore $J^{(s)}$, in terms of $n_0^{(s)}$, $n_N^{(s)}$, and the potentials:

$$J^{(s)}=\nu^{(s)}\exp(-W^{(s)}/k_BT)\times[n_0^{(s)}-n_N^{(s)}\exp(Z^{(s)}eV_N/k_BT)]/S_N^{(s)}. \quad (2.22)$$

The evaluation of the areal densities (called the "concentration profile" in analogy with the continuum case) in the oxide film then follows from (2.20):

$$n_j^{(s)}=(n_0^{(s)}-\zeta^{(s)}S_j^{(s)})\exp(-Z^{(s)}eV_j/k_BT)$$
$$(j=1,2,\cdots,N-1). \quad (2.23)$$

[22] M. J. Dignam, Can. J. Chem. **42**, 1155 (1964).
[23] L. Young, *Anodic Oxide Films* (Academic Press Inc., New York, 1961).
[24] A. T. Fromhold, Jr., J. Phys. Chem. Solids **24**, 1081 (1963).

In the limit of an equilibrium of the sth species (i.e., zero current $J^{(s)}$), $\zeta^{(s)}=0$, and $n_j^{(s)}$ given by (2.23) then reduces to the Poisson-Boltzmann form. Equation (2.22) shows that $J^{(s)}$ is zero whenever the total potential V_N across the film has the particular value $V_{Eq}^{(s)}$,

$$V_{Eq}^{(s)}=(k_BT/Z^{(s)}e)\ln(n_0^{(s)}/n_N^{(s)}). \quad (2.24)$$

This represents the diffusion potential across the film provided by the concentration gradient of the sth species.

The interfacial reactions, considered in the present model to be faster than transport through the oxide, determine the $2r$ interfacial areal densities $n_0^{(s)}$ ($s=1, 2, \cdots, r$) and $n_N^{(s)}$ ($s=1, 2, \cdots, r$). Hence these are considered to be fixed quantities in the subsequent development.

The reason for developing expressions for the particle currents is that the currents determine the rate of particle transport, which in turn limits the rate at which new oxide can be formed. Utilizing the diffusion current equations in the partially summed form, the problem for each given film thickness consists in solving for $N(r+1)$ unknowns, namely, the $J^{(s)}$ ($s=1, 2, \cdots, r$), the $n_k^{(s)}$ ($k=1, 2, \cdots, N-1$; $s=1, 2, \cdots, r$), and the V_k ($k=1, 2, \cdots, N$). Of course, once these quantities are obtained, the σ_k, ($k=1, 2, \cdots, N-1$), E_0, and the E_k ($k=1, 2, \cdots, N$) follow immediately from (2.4), (2.10), and (2.1), respectively. If (2.4) is utilized to eliminate the σ_j in (2.11), then the problem is reduced to obtaining the $N(r+1)$ unknowns listed above from the total of $N(r+1)$ equations given by the $N-1$ equations (2.11) for V_k, the $r(N-1)$ equations (2.23) for $n_j^{(s)}$, the r equations (2.22) for $J^{(s)}$, and an auxiliary relation known as the "coupled currents" requirement. This latter equation is given and discussed in the next subsection.

To obtain a solution, numerical techniques must generally be employed. However, the sums can be evaluated analytically in certain cases, the most noteworthy of which is the "homogeneous field" limit[25] treated in Sec. III.

Coupled Currents

The relation

$$\sum_{s=1}^{r} q^{(s)}J^{(s)}=0 \quad (2.25)$$

is the basis for the coupled-currents approach to thermal oxidation, as contrasted with single-current approaches[15,16] valid in certain limited cases of a current equilibrium. This equation was also utilized by Wagner[6] in his derivation of his parabolic growth law, and, in fact, is almost classical in solid-state physics.[26] It requires that the net electric charge transported through the oxide during any given time increment be zero. The essence of the argument proposed by Wagner for use of this equation is that the growth of a stoichiometric oxide requires the continuous transport of a stoichiometric ratio of particles through the existing film. It can be argued that the zero charge transport situation is intrinsically stable since the field is then unchanged by the particle currents. Equation (2.25) is termed the "kinetic condition"; the potential V_N across the film necessary to satisfy (2.25) is termed the "kinetic potential" to emphasize its role in balancing the currents. Whenever V_N has a value nearly equal to the equilibrium potential (2.24) for one of the currents, the situation is termed[12] growth under a "virtual current equilibrium."

Growth Kinetics

The growth rate of the oxide or other semiconducting or insulating film at a given thickness produced by a given ionic particle current $J^{(s)}$ is given by $R^{(s)}J^{(s)}$, where $R^{(s)}$ is the volume of new oxide formed for each particle of species s which diffuses to the oxide-oxygen interface. If $\Delta L(t)$ denotes a monolayer of oxide and Δt denotes the time necessary to grow this monolayer as determined by diffusion, then $\Delta L(t)/\Delta t$ is the growth rate. If there are l of the total number of r species which are ionic, then the total growth rate of the film is given by summing over these l species:

$$\frac{\Delta L(t)}{\Delta t}=\sum_{s=1}^{l} R^{(s)}J^{(s)}. \quad (2.26)$$

The kinetics of growth [i.e., the oxide film thickness $L(t)$ versus time t] can therefore be obtained using this relation, provided the currents are first evaluated as a function of film thickness according to the procedure outlined in the above subsections.

III. HOMOGENEOUS FIELD LIMIT

The concentrations[12] of diffusing defects in the film as a rule increase exponentially with increasing temperature, as given by a Boltzmann factor, so that the space-charge contributions to the electric field should be largest at high temperatures. At lower temperatures (i.e., within several hundred degrees of ambient temperature), the defect concentrations may be low enough in many cases to neglect space charge. Computations[9] show that defect concentrations of 10^{16} particles/cm^3 or so produce insignificant space-charge contributions to the total electric field until the growing film reaches a thickness of hundreds of angstroms. Therefore the homogeneous field limit, in which all space-charge contributions to the field are neglected relative to the surface charge field E_0, provides a very realistic approximation for oxidation kinetics over a significant range of experimental conditions. This approach is not

[25] A. T. Fromhold, Jr., J. Phys. Chem. Solids **24**, 1309 (1963); Bull. Am. Phys. Soc. **10**, 454 (1965).

[26] N. F. Mott and R. W. Gurney, *Electronic Processes in Ionic Crystals* (Oxford University Press, Oxford, 1940), p. 256.

the same as that of Wagner[6] based on the assumption of charge neutrality, as evidenced by the fact that the rate constants and concentration profiles derived thereby are quite different from those predicted by the Wagner theory.

Homogeneous Field Currents

Equation (2.1) in the homogeneous field limit yields $E_k=E_0$ for all k, while (2.8) yields $V_j=-2ajE_0$ for all j. The total potential V_N across the film is thus $-2aNE_0=-E_0L(t)$ in this limit. The sum $S_j^{(s)}$ of (2.21) becomes a geometric series and can thus be evaluated readily:

$$S_j^{(s)}=\sum_{k=1}^{j}\exp\left(\frac{Z^{(s)}eE_0a(1-2k)}{k_BT}\right)$$
$$=[1-\exp(-2jZ^{(s)}eE_0a/k_BT)]/[2\sinh(Z^{(s)}eE_0a/k_BT)]. \quad (3.1)$$

Utilizing this expression for the particular index $j=N$, and substituting into (2.22), yields the homogeneous field approximation for the particle current:

$$J^{(s)}=2\nu^{(s)}\exp(-W^{(s)}/k_BT)\sinh(Z^{(s)}eE_0a/k_BT)\times[n_N{}^{(s)}-n_0{}^{(s)}\exp(2NZ^{(s)}eE_0a/k_BT)]/[1-\exp(2NZ^{(s)}eE_0a/k_BT)]. \quad (3.2)$$

This expression is identical to Eq. (2.18) of Ref. 17. Substitution of (3.1), (2.18), and (3.2) into (2.23) then yields the areal density profile in the limit of a homogeneous field. It is identical to the profile given by Eq. (4.2) of Ref. 17 in continuum notation, where the areal densities $n_j^{(s)}$ divided by $2a$ yield the corresponding bulk concentrations which are denoted by $C(x)$, with the position x at the potential minimum denoted by index j given by $x=2ja$.

Film Thickness Dependence of Potential

The coupled currents condition (2.25) determines E_0 as a function of $L(t)$. For arbitrary values of $Z^{(s)}$, numerical techniques must still generally be used to obtain a solution. Considerable simplification is effected if all values of $Z^{(s)}$ have the same magnitude, however, because $\sinh(-y)=-\sinh y$ and thus all hyperbolic functions divide out of the coupled-currents equation. For this special case, suppose that the indices $s=1, 2, \cdots, p$ denote species for which $Z^{(s)}=+|Z|$, and suppose $s=p+1, p+2, \cdots, r$ denote species for which $Z^{(s)}=-|Z|$. Let

$$\psi\equiv\exp(2N|Z|eE_0a/k_BT) \quad (3.3)$$

denote a parameter which is independent of s, and define

$$D^{(s)}\equiv 4a^2\nu^{(s)}\exp(-W^{(s)}/k_BT), \quad (3.4)$$

the latter being the generally accepted expression for the diffusion coefficient[17] for the sth species. With these substitutions, the coupled-currents condition (2.25) yields

$$\sum_{s=1}^{p}q^{(s)}D^{(s)}\{n_N{}^{(s)}-n_0{}^{(s)}\psi\}-\sum_{s=p+1}^{r}q^{(s)}D^{(s)}\{n_0{}^{(s)}-n_N{}^{(s)}\psi\}=0. \quad (3.5)$$

Denote the sums by

$$\Gamma_{11}\equiv\sum_{s=1}^{p}q^{(s)}D^{(s)}n_0{}^{(s)}, \quad (3.6)$$

$$\Gamma_{12}\equiv\sum_{s=1}^{p}q^{(s)}D^{(s)}n_N{}^{(s)}, \quad (3.7)$$

$$\Gamma_{21}\equiv\sum_{s=p+1}^{r}q^{(s)}D^{(s)}n_0{}^{(s)}, \quad (3.8)$$

$$\Gamma_{22}\equiv\sum_{s=p+1}^{r}q^{(s)}D^{(s)}n_N{}^{(s)}. \quad (3.9)$$

Equation (3.5) then yields for ψ

$$\psi=(\Gamma_{12}-\Gamma_{21})/(\Gamma_{11}-\Gamma_{22}). \quad (3.10)$$

Referring to the definition of ψ, Eq. (3.3), this relation is noted to give an expression for the homogeneous electric field in the film,

$$E_0=|k_BT/2NZea|\ln[(\Gamma_{12}-\Gamma_{21})/(\Gamma_{11}-\Gamma_{22})]. \quad (3.11)$$

This expression shows that the total potential $V_N=-E_0L(t)=-2aNE_0$ across the film during growth (i.e., the kinetic potential by definition) is a constant, independent of oxide film thickness. Furthermore, for the case of two oppositely charged species only, employment of the Einstein relation and application of the results presented in Appendix A to Eq. (3.11) shows that it gives the same value of the kinetic potential as Eq. (15) of Ref. 27. This is interesting since (3.11) holds for all film thicknesses and corresponding values of the field, while Eq. (15) of Ref. 27 was derived on the basis of the linear-diffusion equation and thus is applicable only in the limit when $Z^{(s)}eE_0a/k_BT$ has a magnitude somewhat less than unity. Therefore, for this particular case of equal magnitudes of $Z^{(s)}$, the potential across the film is not perturbed by nonlinear effects. This is in contrast to the case of unequal magnitudes of $Z^{(s)}$.

A computation of $V_N=-2aNE_0$, utilizing Eq. (3.11) in the limit of two oppositely charged species, has been made as a function of $W^{(1)}-W^{(2)}$, holding all other parameters fixed. Species 1 is considered to have a positive Z value, while $Z^{(2)}$ is considered to be negative. The results, which are presented in Fig. 1, illustrate that

[27] A. T. Fromhold, Jr., J. Chem. Phys. 41, 509 (1964); see also A. T. Fromhold, Jr., J. Phys. Chem. Solids 24, 1309 (1963), especially Sec. 2.

the kinetic potential lies somewhere between the two extremes of an equilibrium potential (2.24) of one or the other of the two species. An increase in $W^{(1)}$ relative to $W^{(2)}$ drives the system toward the negative equlibrium potential, while a decrease in $W^{(1)}$ relative to $W^{(2)}$ drives the system toward the positive equilibrium potential. The fixed parameters utilized for the computations of Fig. 1 are $T=300°\text{K}$, $Z^{(1)}=1$, $Z^{(2)}=-1$, $n_0{}^{(1)}=4\times10^{10}$ particles/cm^2, $n_0{}^{(2)}=1\times10^{10}$ particles/cm^2, $n_N{}^{(1)}=4\times10^7$ particles/cm^2, $n_N{}^{(2)}=1\times10^7$ particles/cm^2, $\nu^{(1)}=10^{12}$/sec, $\nu^{(2)}=10^{15}$/sec, and $a=2$ Å. The results are the same, however, if $n_0{}^{(1)}$, $n_0{}^{(2)}$, $n_N{}^{(1)}$, and $n_N{}^{(2)}$ are multiplied by the same constant factor.

Whenever the $Z^{(s)}$ are of different magnitude for different s, Eq. (3.11) is not valid. In fact, numerical computations[28] utilizing (2.25) and (3.2) show that V_N is significantly dependent on film thickness for thin films, but approaches the constant potential derived in Ref. 27 as soon as the thickness is large enough (generally several tens of angstroms) so that the linear-diffusion equation provides a good approximation. It is noteworthy that no startling difference in the early stage kinetics is observed[28] between the case of the varying early stage potential and the case of the potential which is constant throughout growth.

Kinetics for Constant Potential

Whenever (3.11) is valid so that the value of $V_N=-2aNE_0$ is independent of the film thickness $2aN=L(t)$, then the only term in the homogeneous field current (3.2) which depends on thickness of the oxide is the argument of the hyperbolic sine function. Considering the generally expected case in which each ionic current yields a positive contribution to the growth rate, Eq. (3.2) can be rewritten to yield the following expression for the contribution of each ionic current to the over-all rate:

$$R^{(s)}J^{(s)}=\Lambda^{(s)}\sinh[L_{\text{crit}}/L(t)], \tag{3.12}$$

where

$$L_{\text{crit}}\equiv|ZeaE_0L(t)/k_BT|=|-ZeaV_N/k_BT| \tag{3.13}$$

and

$$\Lambda^{(s)}\equiv|2\nu^{(s)}R^{(s)}\exp(-W^{(s)}/k_BT)\times\{[n_N{}^{(s)}-n_0{}^{(s)}\exp(-ZeV_N/k_BT)]/[1-\exp(-ZeV_N/k_BT)]\}| \tag{3.14}$$

are defined to be positive constants, independent of film thickness.

Equation (3.12) has the same functional form as the Mott-Cabrera equation.[16] The primary difference in the present work (homogeneous field limit) is the mechanism assumed for electron transport (nonlinear diffusion instead of electron tunneling[11] or thermionic emission[12])

[28] Ronald B. Mosley, M.S. Thesis, Auburn University, 1968 (unpublished).

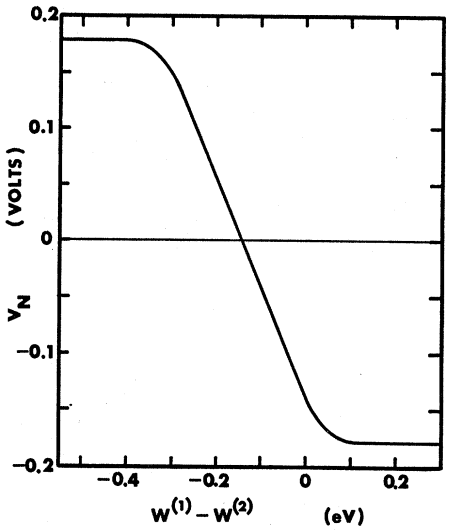

FIG. 1. Electrostatic potential across growing oxide versus the difference in activation energies for the two oppositely charged diffusing species. (Values for parameters are given in text.)

and the resulting manner in which the potential across the film is created and controlled. In the present work, either the ionic or the electronic species can be rate-limiting for growth.

An analytical expression for the growth kinetics can be readily obtained for the present case by approximating the growth rate $\Delta L(t)/\Delta t$ in Eq. (2.26) by the corresponding derivative $dL(t)/dt$. Equations (2.26) and (3.12) then yield

$$\frac{dL(t)}{dt}=\frac{L_{\text{crit}}}{\tau}\sinh\frac{L_{\text{crit}}}{L(t)}, \tag{3.15}$$

where

$$\tau\equiv L_{\text{crit}}/\sum_{s=1}^{l}\Lambda^{(s)}. \tag{3.16}$$

If $L(t)=0$ when $t=0$, this relation can be written as

$$t/\tau=L_{\text{crit}}{}^{-1}\int_0^{L(t)}\operatorname{csch}\left(\frac{L_{\text{crit}}}{\zeta}\right)d\zeta. \tag{3.17}$$

Expansion of the hyperbolic cosecant into the infinite series

$$\operatorname{csch}\frac{L_{\text{crit}}}{\zeta}=2\sum_{m=0}^{\infty}\exp\left(-(2m+1)\frac{L_{\text{crit}}}{\zeta}\right) \tag{3.18}$$

and the change of variable $\xi=L(t)/\zeta$ produce the following exact expression for the oxidation kinetics:

$$t/\tau=2\left(\frac{L(t)}{L_{\text{crit}}}\right)\sum_{m=0}^{\infty}E_2\left(\frac{(2m+1)L_{\text{crit}}}{L(t)}\right). \tag{3.19}$$

Each of the quantities $E_2[(2m+1)L_{\text{crit}}/L(t)]$ is the

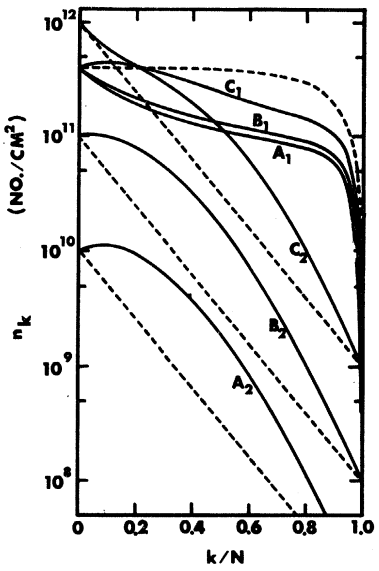

FIG. 2. Monolayer densities of two diffusing species (subscripts 1 and 2) versus position in the oxide. Values of parameters are given in Table I except for variable boundary concentrations of species 2: For curves A, B, and C, $n_0^{(2)}$ has values of 10^{10}, 10^{11}, and 10^{12} particles/cm^2, and $n_N^{(2)}$ has values of 10^7, 10^8, and 10^9 particles/cm^2, respectively. Dashed curves represent zero space-charge limit.

tabulated[29] second-order exponential integral, defined as

$$E_2(\eta)\equiv\int_1^\infty y^{-2}\exp(-\eta y)dy. \tag{3.20}$$

The above series of exponential integrals converges quite rapidly, so that only a few terms are usually needed in Eq. (3.19). For example, the first term alone is sufficient for an accuracy of 1% or better whenever $L(t)<\frac{1}{2}L_{\text{crit}}$. The dimensionless nature of the quantities t/τ and $L(t)/L_{\text{crit}}$ makes it possible to compute a single universal curve (or tabulation)[30] from Eq. (3.19), which can then be used subsequently to obtain $L(t)$ versus t for any particular set of physical parameters.

Parabolic Law

In the limit where $L(t)>L_{\text{crit}}$, which may be as small as 20 Å or so for the present model, the hyperbolic sine function in Eq. (3.15) may be approximated by its argument. Equation (3.15) then reduces to the form

$$\frac{dL(t)}{dt}\simeq\frac{L_{\text{crit}}^2}{\tau}L(t)^{-1}, \tag{3.21}$$

which yields

$$L(t)^2\simeq(2L_{\text{crit}}^2/\tau)t. \tag{3.22}$$

This result is equivalent to the parabolic growth law previously derived by Fromhold[27] on the basis of transport by ions and electrons according to the linear-diffusion equation integrated in the homogeneous field limit. This parabolic growth law differs from the field-controlled parabolic growth law proposed by Cabrera and Mott[16] insofar as concentration gradient effects are included, and it differs from that proposed by Wagner[6] insofar as the defect concentrations at any given point in the oxide for the present model are not generally in stoichiometric ratio.

IV. NONHOMOGENEOUS FIELD COMPUTATIONS

Numerical Techniques

The successive approximation technique, Newton's method, and a time-dependent technique were tried with varying degrees of success for the present numerical solutions. None was completely satisfactory; the numerical treatment of nonlinear equations is difficult and there is presently no general algorithm for their solution. Convergence and stability are the two major properties which constitute the greatest sources of difficulty.

A combination of the steady-state method and the time-dependent method was found to be the best technique regarding both convenience and reliability. It is based on the assumption that the concentration profiles are in the steady state, but the surface-charge field and the number of particles in the growing monolayer are considered to be time-dependent quantities. The steady-state concentrations are used to calculate the corresponding homogeneous currents. These quantities are obtained from a given potential distribution which is time-dependent. The primary difference between this method and that of successive approximation lies in the fact that the surface-charge field is varied between successive approximations for the concentration profiles.

We are confident that the results presented herein are reliable, since each current (including the current for the species in a state of virtual equlibrium) was checked after growth of every monolayer to verify that it was homogeneous throughout the film.[31] This assures self-consistency of the solution at a given thickness. This stringent criterion does limit the scope of the results, since it was found that this condition could not be maintained in the limit of high space charge for thicknesses greater than approximately 75 monolayers. The present results are valuable because they provide a clear and exact picture of the perturbing effects of space charge in the early growth region.

[29] *Handbook of Mathematical Functions*, edited by M. Abramowitz and I. A. Stegun (U. S. Department of Commerce, National Bureau of Standards, Washington, D. C., 1964), Appl. Math. Ser., No. 55, p. 227.

[30] Universal curves and tabulations may be obtained from the authors.

[31] This stringent criterion was not maintained in preliminary numerical computations (Ref. 24, Sec. 3.A), so that the conclusions of the present more comprehensive study are considered to supplant these earlier results.

TABLE I. Parameters for numerical computations. All computations: $\epsilon/\epsilon_0=10$, $R=1.92\times10^{-23}$ cm³, $\nu^{(1)}=10^{12}$/sec, $\nu^{(2)}=10^{15}$/sec, and $Z^{(2)}=-1$.

		Figure											
		2	3	4	5	6	7	8	9	10	11	12	
Symbol	Units											curve *a*	curve *b*
$n_0^{(1)}$	10^{10} particles/cm²	40	40	40	40	40	a	40	40	40	40	4	40
$n_0^{(2)}$	10^{10} particles/cm²	a	a	1	1	1	a	1	1	1	1	1	10
$n_N^{(1)}$	10^{7} particles/cm²	40	40	a	40	40	a	40	40	40	40	4	40
$n_N^{(2)}$	10^{7} particles/cm²	a	a	1	a	1	a	1	1	1	1	1	10
$W^{(1)}$	eV	0.65	0.40	0.65	0.40	a	a	a	a	0.65	0.40	0.65	0.710
$W^{(2)}$	eV	0.55	0.75	0.55	0.75	a	a	a	a	0.55	0.75	0.727	0.787
$Z^{(1)}$	...	1	1	1	1	1	1	1	1	1	1	1	1
a	Å	2	2	2	2	2	2	2	2	2	2	2	2
T	°K	300	300	300	300	300	300	300	a	300	300	300	300

[a] Varied with curve in figure.

Defect Concentration Profiles

The areal densities of the positive and negative diffusing species for three cases in which the negative species (species 2; subscript 2) is near a virtual current equilibrium and the positive species (species 1; subscript 1) is rate-limiting are presented in Fig. 2. The position coordinate (abscissa) is normalized to the film thickness for each curve. For this figure, the thickness N of the film is 20 monolayers. Each monolayer is always chosen to be 4 Å. The values of the parameters utilized for the computations are listed in Table I. These were chosen to be representative of metal-oxide systems in general, but were not chosen for any specific system. For the given activation energies, the results are essentially independent of the type of lattice defects in question. Hence the presently considered negative-gradient case would hold equally well for growth by motion of anion vacancies as it does for growth by motion of cation interstitials. An extension of the numerical results to the positive-gradient case is given in a separate subsection.

The three cases of Fig. 2 correspond to three sets of boundary concentrations for the negative species, while the boundary concentrations of the positive species are held fixed. The curves labeled A_2 and A_1 correspond, respectively, to the negative and positive defect concentrations for the lowest electronic boundary concentrations; the dashed curves represent the corresponding profiles in the limit of a homogeneous field, thus giving an indication of the modification in the profiles introduced by the space charge.

The curves labeled B_2 and B_1 represent the corresponding electronic and ionic areal defect densities when the electronic boundary concentrations are increased by an order of magnitude. The qualitative behavior of the profiles remains unchanged.

The curves labeled C_2 and C_1 represent the corresponding electronic and ionic areal densities when the boundary concentrations of the electronic species are increased still another order of magnitude. The ionic and electronic profiles then cross one another, and the qualitative appearance of the curves is vastly modified.

A companion series of profiles has been computed for three alternate cases in which the positive species (species 1) is near a virtual current equilibrium while the negative species (species 2) is rate-limiting. These are presented in Fig. 3. Again the position coordinate is normalized to the film thickness (20 monolayers). The curves A_2 and A_1 corresponding to electronic and ionic profiles for the lowest ionic boundary concentrations do cross, and thus resemble qualitatively the set C_1 and C_2 of Fig. 2 which also cross. The qualitative behavior of the positive and negative species are noted to be interchanged in Figs. 2 and 3 because the species which is rate-limiting is different in the two figures.

There is no significant qualitative change in the curves A_2 and A_1 in Fig. 3 when the ionic boundary concentrations are increased by an order of magnitude

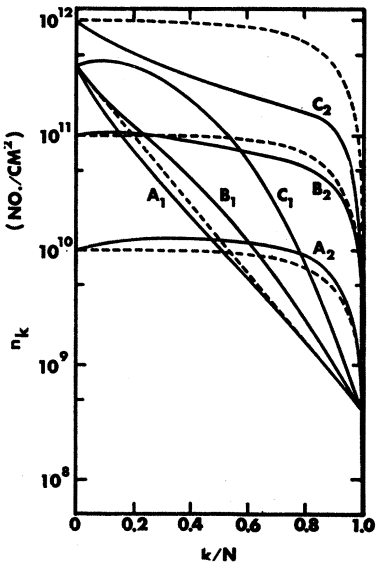

FIG. 3. Monlayer densities of two diffusing species (subscripts 1 and 2) versus position in the oxide. Values of parameters are given in Table I except for variable boundary concentrations of species 2: For curves A, B, and C, $n_0^{(2)}$ has values of 10^{10}, 10^{11}, and 10^{12} particles/cm², and $n_N^{(2)}$ has values of 10^7, 10^8, and 10^9 particles/cm², respectively. Dashed curves represent zero space-charge limit.

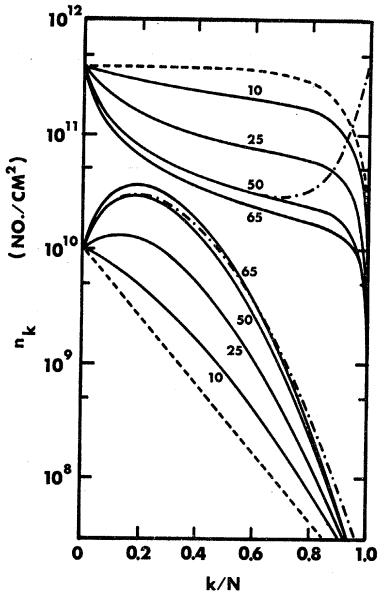

FIG. 4. Monolayer density distributions of two diffusing species in a growing oxide for several values of the film thickness. Dashed curves represent zero space-charge limit of solid curves. Values of parameters are given in Table I except for variable $n_N^{(1)}$, which is 4×10^8 particles/cm^2 for all except dot-dash curve, for which $n_N^{(1)}=n_0^{(1)}$.

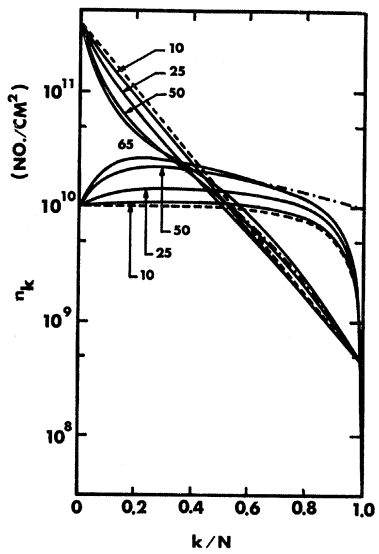

FIG. 5. Monolayer density distributions of two diffusing species in a growing oxide for several values of the film thickness. Dashed curves represent zero space-charge limit of solid curves. Values of parameters are given in Table I except for variable $n_N^{(2)}$, which is 10^7 particles/cm^2 for all except dot-dash curve, for which $n_N^{(2)}=n_0^{(2)}$.

to yield the profiles denoted by B_2 and B_1. A further order-of-magnitude increase in the boundary concentrations, however, yields the uncrossed profiles denoted by C_2 and C_1. These resemble qualitatively the uncrossed profiles of Fig. 2.

The profile of the species near a virtual current-equilibrium is noted in both figures to deviate somewhat from a nearly straight-line behavior on the semi-logarithmic plot, while the profile of the rate-limiting species is somewhat horizontal until it takes a sudden plunge downward near the outer interface. By noting this qualitative behavior, which holds for both the homogeneous-field limit as well as for the computations with space charge, the rate-limiting species can be distinguished.

To summarize, two qualitative types of profile occur, the uncrossed and the crossed. Each can occur for a proper choice of relative ionic and electronic defect concentrations, and thus the characteristic does not depend critically on which species is rate-limiting.

Figure 4 illustrates the variation of the areal defect densities with film thickness. The curves represent a case in which the profiles are uncrossed, namely, the pair of curves A_2 and A_1 in Fig. 2. The position coordinate is normalized to the film thickness for each curve, with the thickness in monolayers given on each curve. The upper curves in the figure represent the ionic defect profile, while the lower curves represent the electronic defect profile. Note that the profiles of the negative and positive species pull closer and closer together for the thicker films, corresponding to a tendency for the space charge to neutralize partially in the interior of the film. The dashed curves again represent the corresponding profiles in the limit of a homogeneous field. The dot-dashed curves in Fig. 4 (and also in Fig. 5) illustrate the effect of perturbing the outer boundary concentration of the rate-limiting species; such effects are discussed under "Ohmic Transport."

Figure 5 illustrates the corresponding variation of the areal defect densities with film thickness for the case in which the profiles are crossed. This sequence of curves corresponds to the pair of curves A_2 and A_1 in Fig. 3, for which the electronic species is rate-limiting. In referring to these figures, it is helpful to remember that in both Figs. 4 and 5 the ionic boundary concentration at the metal-oxide interface ($x=0$) is larger than that for the electronic species. The tendency toward space-charge neutralization with increasing film thickness in Fig. 5 for the crossed profile case is much less pronounced than for the uncrossed profile case of Fig. 4, since a profile crossing already represents a partial neutralization of the space charge.

The dashed curves in Figs. 4 and 5, which represent the corresponding homogeneous field profiles for each of the cases, are independent of film thickness on the normalized plots. The homogeneous field curves serve the purpose of illustrating the modifications of the profiles introduced by the space charge. Some insight into the reasons for the difficulty in obtaining an exact analytical solution to the present problem can be attained by noting the contortions of the curves in Figs. 4 and 5 as the space charge in the film increases. Previous numerical computations[32] have also illustrated

[32] A. T. Fromhold, Jr., J. Chem. Phys. 39, 2278 (1963).

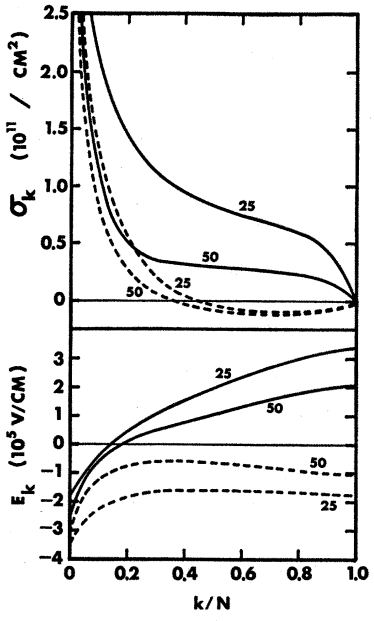

FIG. 6. Space-charge monolayer density and electric field as a function of normalized position in the growing oxide. The solid curves represent two thicknesses (25 and 50 monolayers) with activation energies $W^{(1)}=0.65$ and $W^{(2)}=0.55$ eV; the dashed curves represent corresponding computations with $W^{(1)}=0.40$ and $W^{(2)}=0.75$ eV. Other parameters are given in Table I.

this feature; the present numerical computations, however, are the first which have been made subject to the condition of balanced currents given by Eq. (2.25).

Space Charge and Electric Field Distributions

Other features of the computations of Figs. 4 and 5 are now illustrated. The upper curves in Fig. 6 illustrate the space-charge profile across the film, while the lower curves in Fig. 6 illustrate the electric-field variation with position in the film. Again the position in the film is normalized to the film thickness. Curves are given for different thicknesses; the thickness in monolayers is given on each curve. The solid curves represent the uncrossed-profile case corresponding to Fig. 4, while the dashed curves represent the crossed-profile case corresponding to Fig. 5. It is noted in Fig. 6 that the sign of the space charge is positive throughout the film for the uncrossed-profile case, while the sign of the space charge reverses inside the film for the crossed-profile case.

The most striking feature of the space-charge profiles σ_k is the decreasing concentration of charge in the latter 80% or so of the film as the film thickness increases. This effect, which is especially pronounced for values of N less than 25 monolayers (not shown in Fig. 6), is due in part to an initial increase in total space charge with film thickness. The curves for the electric field in the lower part of Fig. 6 illustrate that the fields become more and more inhomogeneous as the thickness increases. Note that the values of the electric field are in the range of 10^5 V/cm.

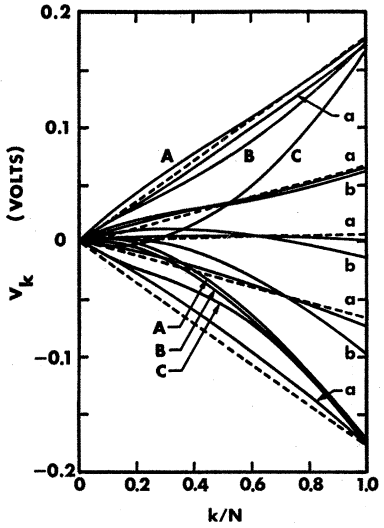

FIG. 7. Electrostatic potential as a function of position in the growing oxide film. The five groups of curves have values of V_N in the homogeneous-field limit of 0.178, 0.067, 0.007, −0.065, and −0.178 V, corresponding, respectively, to values for $W^{(1)}-W^{(2)}$ of −0.35, −0.21, −0.15, −0.077, and +0.10 eV. Table I lists values for fixed parameters. The curves labeled A, B, C, a, b in the several groups have the following boundary concentrations:

		Curves			
Parameters	Units	A	B, b	C	a
$n_0^{(1)}$	10^{10}/cm^2	40	40	40	4
$n_0^{(2)}$	10^{10}/cm^2	1	10	100	1
$n_N^{(1)}$	10^7/cm^2	40	40	40	4
$n_N^{(2)}$	10^7/cm^2	1	10	100	1

Potential Distributions

The variation of electrostatic potential with position in the film for $N=20$ monolayers is shown in Fig. 7 for all six individual cases illustrated in Figs. 2 and 3 and for intermediate potential cases. The lower curves (i.e., negative potential) labeled A, B, and C correspond, respectively, to the cases labeled A, B, and C in Fig. 2, where the ionic species is rate-limiting. The upper curves (i.e., positive potential) labeled A, B, and C correspond to the cases labeled in the same manner in Fig. 3, where the electronic species is rate-limiting.

The upper and lower curves labeled by the letter a illustrate the change in the corresponding curves labeled B when all four boundary concentrations are lowered by an order of magnitude to decrease the space charge in the film.

The intermediate-potential cases were chosen with the aid of Fig. 1; each case is given for two values of boundary concentrations (curves a and b in each set) differing by an order of magnitude. All curves labeled a in Fig. 7 have the same boundary concentrations, while all curves labeled b (or B) have boundary concentrations an order of magnitude higher.

Note that the potential *at the outer interface* differs appreciably for the pair a, b for the intermediate cases; this is in contrast with the pair a, B in the upper and lower sets of curves, which represent cases of growth

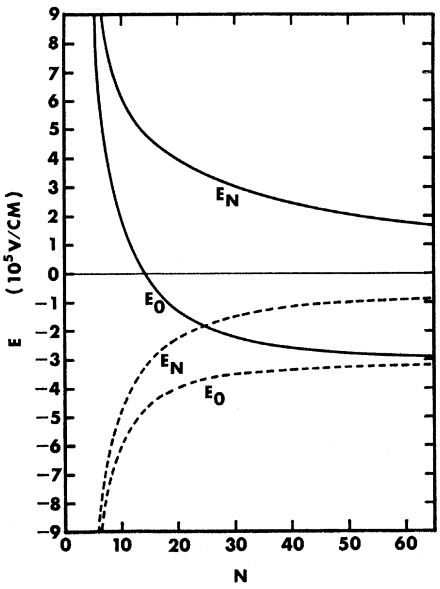

FIG. 8. Electric fields E_0 and E_N at the inner and outer interfaces of the oxide versus the thickness in monolayers. The solid curves represent computations with $W^{(1)}=0.65$ and $W^{(2)}=0.55$ eV; the dashed curves represent computations with $W^{(1)}=0.40$ and $W^{(2)}=0.75$ eV. Values of other parameters are given in Table I.

under conditions near a virtual current equilibrium. For these latter cases, the kinetic potential is very nearly independent of space-charge concentration and film thickness. This is an important observation as regards any approximate treatment of space-charge effects,[8–10] since it is generally necessary to make some assumption regarding either the total potential or the surface-charge field.

The dashed curves in Fig. 7 represent the linear variation of the potential with position appropriate for the homogeneous-field case. The curves for the nonhomogeneous-field case are noted to depart more and more from a linear function with increasing space charge. The thickness dependence (not illustrated) of the potential curves, with potential plotted versus position in the film as normalized to the thickness, is very similar for any given case to the trend illustrated in Fig. 7 for which N is fixed at 20 monolayers and space-charge magnitude is the variable.

Surface-Charge Fields

Figure 8 shows the dependence of the electric field E_0 at the metal-oxide interface and the electric field E_N at the oxide-oxygen interface on the thickness N of the film in monolayers for the numerical computations leading to Figs. 4 and 5. The solid and dashed curves correspond, respectively, to the computations of Figs. 4 and 5. The most striking feature is the asymptotic convergence of E_0 toward some fixed value as N increases for both the uncrossed profile case (solid curve) and the crossed profile case (dashed curve). The behavior of E_N is noted to be similar, but not so pronounced. The two computations corresponding to Figs. 4 and 5 are based on the same values for the boundary concentrations, but widely differing mobilities. The asymptotic approach of the interfacial electric fields toward some fixed value which is the same for the two cases is therefore a feature which occurs because of the choice of equal boundary concentrations and despite the widely differing mobilities. Hence this asymptotic limit must represent the zero-growth-rate case in which the currents for all practical purposes are zero. The system characterized by such a field would be in a state of chemical equilibrium, and no further change in film thickness would be possible.

Total Space Charge; Space-Charge Modified Currents

Other features of the same computations leading to Figs. 4 and 5 are illustrated in Fig. 9. The upper curves give the total space charge σ_{tot} in the film as a function of thickness of the film, where σ_{tot} is defined as the total charge in the film due to the positive species minus the magnitude of the total charge in the film due to the negative species. The uncrossed-profile case is illustrated by the solid curve while the crossed-profile case is illustrated by the dashed curve. The crossed-profile curve lies considerably below the uncrossed-profile case, illustrating the fact that a profile crossing represents a partial neutralization of the total space charge. It can be seen that σ_{tot} for the uncrossed-profile case goes through a maximum (thickness range of 20–25 monolayers), and then gently decreases with increasing thickness.

The dot-dashed curve for σ_{tot} corresponds to a higher temperature computation (600°K instead of 300°K), with all values of the remaining parameters chosen to have the same values as were used in computing the solid curve. These results are discussed under "Temperature Dependence."

The lower curves in Fig. 9 illustrate the film-thickness dependence of the difference $(J_{NSC}-J_{SC})$ between the particle current J_{NSC} computed for a homogeneous field and the particle current J_{SC} computed including space charge. The quantity $J_{NSC}-J_{SC}$ can thus be considered to be proportional to the change or modification in the current due to the perturbing effect of space charge. The values are normalized to the corresponding value of J_{NSC} for $N=25$ monolayers (designated as J_{NSC}^{25}), so that the ordinate of the curves in the bottom of Fig. 9 is dimensionless. The solid curve (for which $J_{NSC}^{25}=1.27\times10^{12}$ particles/cm² sec) again represents the uncrossed-profile case corresponding to Fig. 4, while the dashed curve (for which $J_{NSC}^{25}=7.21\times10^{11}$ particles/cm² sec) represents the crossed-profile case corresponding to Fig. 5. The dot-dashed curve (for which $J_{NSC}^{25}=2.91\times10^{17}$ particles/cm² sec) again corresponds to the higher-temperature case. The curves designated by long and short dashes are $\pm J_{NSC}$ curves, again normalized to J_{NSC}^{25}; the upper one corresponds to the solid $(J_{NSC}-J_{SC})$ curve, while the lower one corresponds to

the dashed ($J_{NSC}-J_{SC}$) curve. For $N>30$ monolayers, the curves $\pm J_{NSC}$ vary nearly inversely with film thickness, corresponding to parabolic growth; comparison of the slope of a ($J_{NSC}-J_{SC}$) curve with the corresponding slope of the J_{NSC} curve at a given film thickness gives a good indication of how much the space charge is perturbing the growth kinetics from the parabolic form at that particular thickness. Note that the deviations are very large in the early growth period. Additional information concerning the kinetics is given in subsequent figures.

The sign and magnitude of the ($J_{NSC}-J_{SC}$) curves are also of importance. The sign for the solid curve (lower part of Fig. 9) is positive, corresponding to a smaller current with space charge than without space charge. Thus the growth rate is retarded by the space charge for this case. It is interesting that this curve rises almost linearly for thin films, and then levels off. This is in agreement with the predictions of first-order[8,10] and second-order[10] perturbation treatments, respectively. Subsequent to the leveling off, the curve decreases gently with increasing thickness, but the slope is less than that of an inverse thickness dependence, as seen by comparison with the corresponding J_{NSC} curve. There is a definite correlation between the shape of the solid curves for σ_{tot} and $J_{NSC}-J_{SC}$.

The dashed curve for $J_{NSC}-J_{SC}$ at the bottom of Fig. 9 is negative, corresponding to a larger current with space charge than without space charge. Thus the growth rate is enhanced by space charge for this case. Again the curve initially increases in value with increasing N, but then levels off. Note that even for the largest values of N, the slope is still significantly different from that of the corresponding $-J_{NSC}$ curve. The correlation between the shape of the dashed curves for σ_{tot} and $J_{NSC}-J_{SC}$ is again evident, but in this case the signs for σ_{tot} and $J_{NSC}-J_{SC}$ are opposite. This is due to the fact (as discussed later) that the sign of the total space charge is the same for the two cases while the sign of the defect species which limits the growth rate is opposite for the two cases.

The correlation between the curves for σ_{tot} and $J_{NSC}-J_{SC}$ noted in Fig. 9 holds not only for the shape of the curves, but also for magnitude of the curves. For both σ_{tot} and $J_{NSC}-J_{SC}$, the magnitudes of the solid curves are larger than the magnitude of the dashed curves. Thus the total space charge in the film determines the degree to which the current is perturbed from the zero-space-charge case. This agrees with the predictions of the averaging technique.[9]

The dependence of the quantity J_{SC}/J_{NSC} with thickness (not shown in figures) is of some interest, since it is complementary to the curves in the lower part of Fig. 9. This quantity, representing the ratio of the current as computed including space-charge effects to the current as computed in the homogeneous field limit, starts out at zero thickness with the value unity. It decreased monotonically with increasing N for the

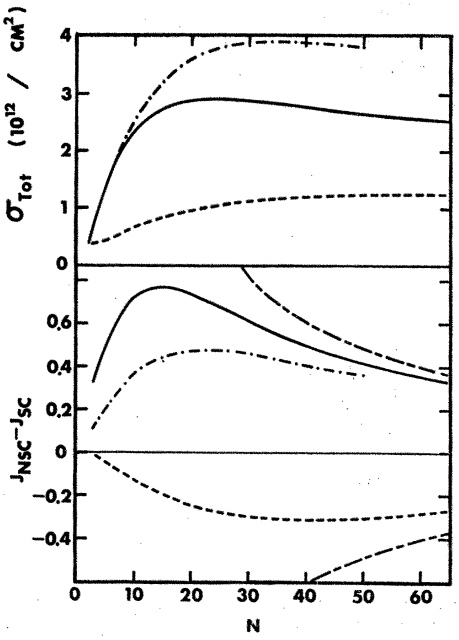

FIG. 9. Total space charge and corresponding relative deviation in particle current from homogeneous-field value as a function of thickness (in monolayers) of the growing oxide. All curves except the dot-dash curve represent a temperature of 300°K; the dot-dash curve is for $T=600$°K. (Solid and dot-dashed curves: $W^{(1)}=0.65$ and $W^{(2)}=0.55$ eV. Dashed curves: $W^{(1)}=0.40$ and $W^{(2)}=0.75$ eV.) The long-dash–short-dash curves in the lower half of the figure represent zero space-charge curves, as further explained in the text. Table I lists values of the remaining parameters.

uncrossed-profile case (Fig. 4), reaching a value of 0.118 at 65 monolayers. [At this point, $J_{SC}=5.57\times10^{10}$ particles/cm^2 sec, $J_{NSC}=4.74\times10^{11}$ particles/cm^2 sec, $J_{NSC}-J_{SC}=4.18\times10^{11}$ particles/cm^2 sec, $(J_{NSC}-J_{SC})/J_{NSC}^{25}=0.330$, and $J_{NSC}/J_{NSC}^{25}=0.374$.] On the other hand, for the crossed-profile case (Fig. 5) the quantity increases monotonically with increasing N, reaching a value of 1.74 at 65 monolayers. [At this point, $J_{SC}=4.69\times10^{11}$ particles/cm^2 sec, $J_{NSC}=2.70\times10^{11}$ particles/cm^2 sec, $J_{NSC}-J_{SC}=-2.00\times10^{11}$ particles/cm^2 sec, $(J_{NSC}-J_{SC})/J_{NSC}^{25}=-0.277$, and $J_{NSC}/J_{NSC}^{25}=0.374$.] It would be very worthwhile to compute σ_{tot} and $J_{NSC}-J_{SC}$ for even greater thicknesses to find out the ultimate film-thickness dependence of these quantities. Unfortunately, this could not be done with the numerical scheme utilized for the present studies, as mentioned in the "Numerical Techniques" subsection.

Kinetics

Figures 10 and 11 illustrate results obtained for film thickness versus time (lower curves) and kinetic potential versus time (upper curves). To point out the effects of space charge, a comparison is given in the figures between the nonhomogeneous field results (solid curves) and the corresponding curves (dashed) based on the homogeneous-field approximation. The

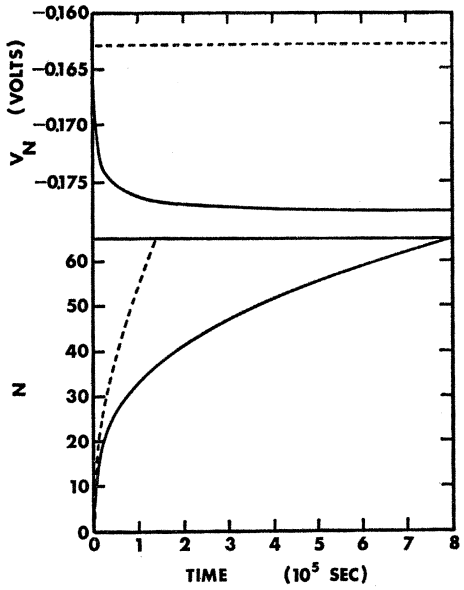

FIG. 10. Electrostatic potential across growing oxide and film thickness in monolayers versus time of oxidation. Dashed curves representing the zero space-charge limit illustrate that space charge retards growth rate for this case. Values for parameters are listed in Table I.

homogeneous-field results were computed according to the formulation given in Sec. III using identical values for the parameters as were utilized for the computations including space-charge effects. The curves in Figs. 10 and 11 correspond, respectively, to the computations of Figs. 4 and 5. Figures 10 and 11 illustrate two possible effects of space charge on growth rate: In certain cases the rate is retarded by space charge, as illustrated in Fig. 10, but in other cases the rate is enhanced by space charge, as illustrated in Fig. 11.

The kinetic potential V_N can be observed in Fig. 10 to depend somewhat on time (and hence on film thickness), while in Fig. 11, it is almost time-independent. The corresponding potentials in the homogeneous-field approximation are rigorously time-independent, since the magnitudes of $Z^{(1)}$ and $Z^{(2)}$ for these curves are equal ($Z^{(1)}=1$, $Z^{(2)}=-1$). The result illustrated of a nonconstant kinetic potential whenever space-charge effects are important appears to be quite general. The variation can be quite small whenever either current is near a virtual equilibrium, as is the case for Figs. 10 and 11, but can be relatively large when neither current approaches a virtual equilibrium.

In Fig. 10, the system is near the state of a virtual electronic current equilibrium, while in Fig. 11 the system is near the state of a virtual ionic current equilibrium. The state of the system with respect to a current equilibrium is one important factor in determining whether growth is retarded or enhanced by space charge; the other equally important factor has been found to be the sign of the space charge. In Fig. 10, the rate-limiting species is ionic, since the system is near a virtual electronic current equilibrium; the space charge itself is predominantly ionic, as illustrated by the upper solid curve for σ_{tot} in Fig. 9. The rate-limiting species and the predominant space charge thus are of the same sign, and the growth rate is found to be retarded.

In Fig. 11, on the other hand, the rate-limiting species is electronic, since the system is near a virtual ionic current equilibrium, while the space charge is still predominantly ionic, as illustrated by the upper dashed curve for σ_{tot} in Fig. 9. The rate-limiting species and the predominant space charge thus are of opposite sign, and the growth rate is found to be enhanced.

The effects of the correlation noted in Fig. 9, that the magnitude of the perturbing effects of space charge on the current depends on the total space charge in the film, can be seen quite distinctly by comparing Figs. 10 and 11. The magnitude of the deviation of lower solid curves from the dashed curves is much larger for Fig. 10 (uncrossed profiles; relatively large σ_{tot}) than for Fig. 11 (crossed profiles; smaller σ_{tot}). Similarly, the deviation of the kinetic potential V_N from the homogeneous-field limit can be seen to be larger in Fig. 10 than in Fig. 11.

The functional form of the film thickness-versus-time curves for Figs. 10 and 11 is of interest. Plots (not shown) of logarithm of film thickness versus logarithm of time were made for each growth curve, including those for the homogeneous-field limit. The slopes of the straight-line portions of such curves gave values for the parameter n, where $L(t) \propto t^{1/n}$ represents an empirical description of the growth curve. The homogeneous field growth curves for thicknesses greater than 25 monolayers were essentially parabolic (i.e., straight line with

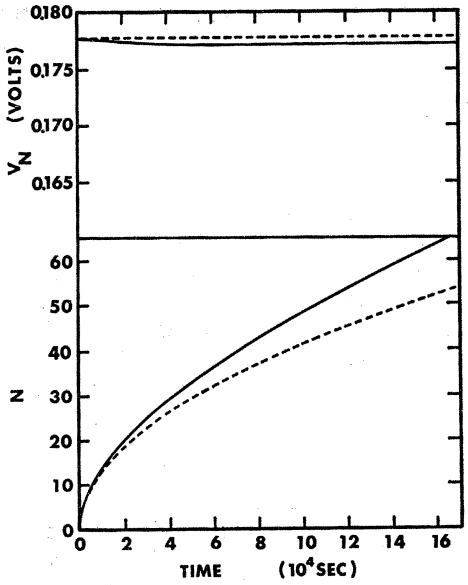

FIG. 11. Electrostatic potential across growing oxide and film thickness in monolayers versus time of oxidation. Dashed curves representing the zero space-charge limit illustrate that space charge enhances growth rate for this case. Values of parameters are listed in Table I.

slope of 2 on the log-log plot), since nonlinear effects were inappreciable in this thickness range. The value of n was of course larger in the thin-film region due to nonlinear effects, varying from approximately 2.2 to 4.4 at a thickness of five monolayers for the series of computations which were performed.

The growth curve including space-charge effects in Fig. 10 for $N>18$ monolayers was found to approximate a straight line with $n=3.04$; a slope of 3 would correspond to a cubic growth law $L(t)^3 \propto t$, so the computed growth curve can be said to be "pseudocubic." This growth law is in agreement with recent analytical work.[33] The several other curves in the series representing retarding effects of space charge computed in the present study had values of n which ranged between 2.2 and 3.0. The limiting-thickness type of nth-root growth laws as produced by space-charge effects thus appears to have a sound theoretical basis.

Figure 11 represents a case in which space charge enhances the growth rate; for $N>25$ monolayers, this curve on the log-log plot was found to approximate a straight line with a slope of 1.75. Since a slope of 2 corresponds to parabolic growth, while a slope of one corresponds to linear growth $[L(t) \propto t]$, the computed growth curve can be said to be "paralinear."

Figure 12 illustrates kinetics for growth under conditions far removed from those necessary for a virtual current equilibrium of either species. Curves a and b correspond, respectively, to the pair of negative potential curves a and b in Fig. 7 which have values of V_k at $k=N$ between -0.06 and -0.10 V; they lie above the lowest set which represent a virtual electronic current equilibrium. Curve b represents an increase in all four boundary concentrations by an order of magnitude relative to those of curve a, with a corresponding decrease of the mobilities for both species by an order of magnitude. As noted in Fig. 7, there is a considerable difference in V_k at $k=N$ for curves a and b; this is reflected also in the time dependence of V_N given in the upper curves of Fig. 12. The potential changes with time by a factor of nearly 2 in Fig. 12, whereas the corresponding changes of the potential

TABLE II. Time in minutes to reach 20 monolayers.

Curve	Figure 2[a] Without space charge	Figure 2[a] With space charge	Figure 3[b] Without space charge	Figure 3[b] With space charge
A	212	376	371	336[c]
B	195	342	38.6	41.3
C	191	256	4.71	9.11

[a] Ions rate-limiting; electrons near a virtual current equilibrium; $W^{(1)}=0.65$ eV, $W^{(2)}=0.55$ eV.
[b] Electrons rate-limiting; ions near a virtual current equilibrium; $W^{(1)}=0.40$ eV, $W^{(2)}=0.75$ eV.
[c] Note that growth is enhanced by space charge for this case; for the other five cases listed, growth can be noted to be retarded by space charge.

[33] K. Hauffe, L. Pethe, R. Schmidt, and S. R. Morrison, J. Electrochem. Soc. 115, 456 (1968).

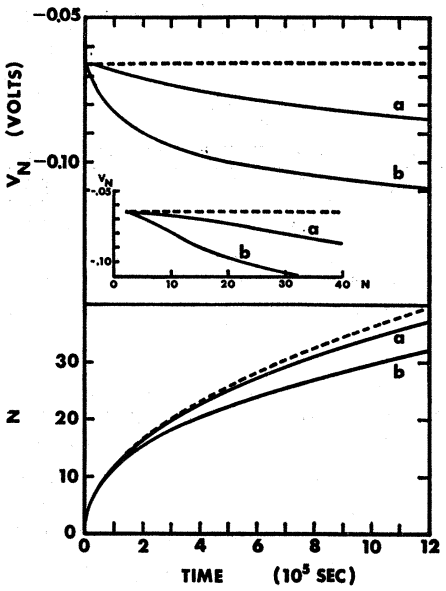

FIG. 12. Electrostatic potential across growing oxide and film thickness in monolayers versus time of oxidation for two values of space charge differing by an order of magnitude. Inset illustrates potential versus monolayer number. Values for parameters are listed in Table I.

with time in Figs. 10 and 11 are less than 10%. The time dependence of the potential for the nonhomogeneous-field case is always found to be significantly larger when the system is not in a virtual current-equilibrium state.

The inset in the upper half of Fig. 12 gives V_N versus N. Note that the deviation from the dashed curve in the inset giving the value of V_N in the homogeneous-field limit is considerably larger for curve b than for curve a, due to the fact that the space charge is larger for curve b than for curve a.

The film-growth curve b in Fig. 12 departs more from the dashed curve representing the homogeneous-field limit than does curve a, again reflecting the effects of the larger space-charge concentrations for curve b. Since the product of mobility and concentration was chosen to have the same value for curves a and b, the same dashed curve represents the homogeneous-field limit for both. The deviation of the solid curves from the dashed curves thus accurately reflects the effects of space charge on the growth kinetics.

Empirical Correlation between Total Space Charge and Growth Rate

Table II summarizes our results for time of growth of 20 monolayers for a series of computations corresponding to all six cases illustrated in Figs. 2 and 3. A relative comparison between the numbers in the table for the time of growth yields all the worthwhile information; the values themselves are not of fundamental significance, since they scale linearly with mobility as long as a constant ratio is maintained between the two

TABLE III. Total space charge at 20 monolayers in units of $10^{11}/cm^2$.

	Figure 2			Figure 3		
Curve	Profile[a]	σ_{tot}	Rate-limiting species	Profile[a]	σ_{tot}	Rate-limiting species
A	*O*	28.7	+	*X*	9.41[b]	−
B	*O*	25.8	+	*X*	−0.569	−
C	*X*	5.55	+	*O*	−35.2	−

[a] The crossed-profile cases are denoted by *X*; the uncrossed-profile cases are denoted by *O*.
[b] This case is the only one of the six in which the product of the sign of the total space charge and the sign of the rate-limiting species is negative.

mobilities. (A constant ratio between mobilities is equivalent to a variation in both $W^{(1)}$ and $W^{(2)}$ subject to the condition of a fixed value for $W^{(1)}-W^{(2)}$.) With this type of scaling, the concentration profiles are unperturbed, so that the distribution of space charge in the film, the electric fields, and the potentials are unchanged. It is noted in Table II that the three computations relevant for Fig. 2 yield times which are of the same order of magnitude, while those relevant for Fig. 3 yield times which differ sequentially by roughly an order of magnitude. These differences are readily explained. For Fig. 2, the ions are rate-limiting in each case; since the ionic mobility and the largest ionic boundary concentration are held fixed for the three computations, the product (i.e., the ionic conductivity) is unchanged and the times of growth are of the same order of magnitude. They differ in the zero space-charge limit only because of slightly different kinetic potentials (V_N has values in the homogeneous-field limit of −0.163, −0.177, and −0.178 V, respectively, for curves *A*, *B*, and *C* of Fig. 2). For Fig. 3, the electrons are rate-limiting in each case; the electronic mobility is held fixed but the largest electronic boundary concentration is increased successively by an order of magnitude for each of the three computations, so that the product (i.e., the electronic conductivity) increases successively by an order of magnitude for each of the three computations. Thus the times of growth decrease successively by roughly an order of magnitude, differing from this exact figure in the zero space-charge limit only because of slightly differing kinetic potentials (V_N has values in the homogeneous field limit of 0.178, 0.171, and 0.141 V, respectively, for curves *A*, *B*, and *C* of Fig. 3).

Table III summarizes the corresponding values of total space charge in the film for the six cases discussed above. Note the correlation which exists between the magnitude of σ_{tot} and the type of profile, the space-charge magnitude being larger for the case of uncrossed profiles than for the crossed profiles.

The sign of the rate-limiting species is also listed in Table III for each of the six cases. The rate-limiting species is considered to be that species for which transport is aided by the kinetic potential across the film; for the presently considered case of diffusion from the metal-oxide interface to the oxide-oxygen interface, this is the species with the sign opposite to the sign of the kinetic potential. The product of the sign of the rate-limiting species and the sign of the total charge is noted to be positive for every case in Table III except for the case of curve *A* of Fig. 3; a comparison with Table II shows that this case is also the only one of the six for which enhanced growth occurs.

The correlation between the product of the signs of the total space charge and the rate-limiting species and the effect of space charge on growth kinetics is further developed in Table IV. Kinetic potentials for each of the curves in Fig. 7 are listed, together with information regarding type of profile, magnitude and sign of total space charge at 20 monolayers, and the ratio of the growth time t_{SC} including space charge to the growth time t_{NSC} in the homogeneous-field approximation. Ratios t_{SC}/t_{NSC} greater than 1 correspond to retarded growth, while ratios less than 1 represent enhanced growth. Utilizing the fact that the sign of the rate-limiting species is opposite to that of V_N for the presently considered cases, the sign obtained by taking the product of that of the total space charge and the rate-limiting species is computed and listed in Table IV. In every case, it is seen that this sign is positive for $t_{SC}/t_{NSC}>1$, representing retarded growth, while it is seen to be negative for $t_{SC}/t_{NSC}<1$, representing enhanced growth. Furthermore, this correlation has been verified for all other computations which have been made to date, including 11 calculations designed to study special effects such as perturbations resulting from variation of individual parameters. On the basis of this correlation, we propose our first empirical rule for space-charge effects: *Space charge retards the growth rate whenever the sign of the rate-limiting species is the*

TABLE IV. Correlation between space-charge retardation or enhancement of growth rate and the product of the sign of rate-limiting species and the sign of the total space charge in the film for all computations of Fig. 7.

Curve	Profile	σ_{tot} ($10^{11}/cm^2$)	V_N(V)[a]	Product of signs[b]	(t_{SC}/t_{NSC})[c]
a	*X*	−0.27	0.172	+	1.01
A	*X*	9.41	0.178	−	0.91
B	*X*	−0.57	0.173	+	1.07
C	*O*	−35.2	0.167	+	1.93
a	*X*	1.06	0.066	−	0.991
b	*X*	6.73	0.063	−	0.95
a	*O*	2.43	0.002	−	0.998
b[d]	*O*	13.4	−0.014	+	1.015
a	*O*	4.02	−0.073	+	1.04
b	*O*	20.4	−0.097	+	1.30
A	*O*	28.7	−0.174	+	1.77
B	*O*	25.8	−0.178	+	1.75
C	*X*	5.55	−0.179	+	1.34
a	*O*	5.32	−0.177	+	1.10

[a] Kinetic potential at 20 monolayers including the effects of space charge.
[b] Product of sign of total space charge and sign of charge of rate-limiting species.
[c] Ratio greater than 1 indicates retarded growth; ratio less than 1 indicates enhanced growth.
[d] Electric fields as large as 10^5 V/cm inside film; field is negative in first part of film but positive in latter part of film.

same as the sign of the total space charge in the film; space charge enhances the growth rate whenever the sign of the rate-limiting species is opposite to the sign of the total space charge in the film.

It should be pointed out in connection with this empirical rule that in some cases the total space charge undergoes a change in sign during growth. This occurs, for example, in curve B of Fig. 3, where σ_{tot} is positive for $N<10$ monolayers, but is negative from 10 to 20 monolayers. The space-charge effects relevant for the latter growth stage predominate, however, as evidenced by the fact that the over-all effect is throughout growth one of retardation (curve B with $V_N=0.173$ V in Table IV). Thus the early stage growth for this case is an example in which the above empirical rule does not hold.

Analytical verification of the rule is possible for cases where the following two conditions are met: (a) the non-rate-limiting species is near a virtual current equilibrium, so that V_N is essentially unperturbed by the space charge, and (b) the space-charge density does not undergo a sign change within the film. The first of these conditions, together with the convention $V_0=0$, allows us to interpret the term $(m/N)(V_N-V_0)$ occurring in Eq. (2.11) as the homogeneous-field potential V_m^0 at the mth potential well. The non-homogeneous-field potential V_m at the mth potential well given by Eq. (2.11) then becomes

$$V_m=V_m^0+\delta V_m, \tag{4.1}$$

where

$$\delta V_m=\left(1-\frac{m}{N}\right)\sum_{j=0}^{m-1} j\sigma_j+m\sum_{j=m}^{N-1}\left(1-\frac{j}{N}\right)\sigma_j. \tag{4.2}$$

The second of the above conditions allows us to conclude that the sign of δV_m in Eq. (4.2) is the same as the sign of the space charge σ_j, since both j and m are equal to or less than N.

The ratio of the current J_{SC} of a given species to the corresponding current J_{NSC} in the homogeneous-field limit can be obtained from Eq. (2.22); the first of the above conditions reduces this ratio to the following simple form:

$$J_{\text{SC}}/J_{\text{NSC}}=S_N^0/S_N, \tag{4.3}$$

where S_N is given by Eq. (2.21) for this species in question, and S_N^0 is the same quantity evaluated in the homogeneous-field limit. Substitution of Eq. (4.1) into Eq. (2.21) yields the following expression for Eq. (4.3):

$$\frac{J_{\text{SC}}}{J_{\text{NSC}}}=\sum_{k=1}^{N}\exp\left(\frac{Ze(V_{k-1}^0+V_k^0)}{2k_BT}\right)\Bigg/ \sum_{k=1}^{N}\left[\exp\left(\frac{Ze(V_{k-1}^0+V_k^0)}{2k_BT}\right)\times\exp\left(\frac{Ze(\delta V_{k-1}+\delta V_k)}{2k_BT}\right)\right]. \tag{4.4}$$

This equation is valid for any diffusing species in the film. Application to the rate-limiting species and use of the fact that δV_k has the sign of the space charge yields the immediate result that $J_{\text{SC}}/J_{\text{NSC}}$ is less than 1 when the sign of the rate-limiting species is the same as the sign of the net space charge, but greater than 1 when the sign of the rate-limiting species is opposite to the sign of the net space charge. Thus the above empirical rule is verified analytically for such conditions, and therefore can be said to be semiempirical.

Examination of the values of V_N in Table IV (or Fig. 7) shows values which fall into five groups, namely, values in the neighborhood of 0.17, 0.06, 0.01, -0.08, and -0.18 V. The four cases for which $V_N\simeq 0.17$ V illustrate an excellent correlation between the magnitude of σ_{tot} and the deviation of $t_{\text{SC}}/t_{\text{NSC}}$ from a value of 1. In every case, the larger values of σ_{tot} result in a larger retardation or enhancement, as the case may be, of growth rate. Note also the same correlation for the two cases for which $V_N\simeq 0.06$ V, for the two cases in which $V_N\simeq 0.01$, for the two cases in which $V_N\simeq -0.08$, and for the four cases in which $V_N\simeq -0.18$ V. This leads us to propose our second empirical rule for space-charge effects: *For a given kinetic potential, the extent to which the growth rate is modified by space charge is qualitatively proportional to the total space charge in the film, which in turn depends on the boundary concentrations and the character of the concentration profiles.* The dependence of rate on total space charge is in agreement with predictions based on the averaging technique.[9] In addition, Eq. (4.2) shows that δV_m increases in magnitude with the magnitudes of σ_j; this in turn yields a larger deviation of the ratio $J_{\text{SC}}/J_{\text{NSC}}$ in Eq. (4.4) from the value of 1. Therefore under the same conditions of constant V_N and a uniform sign for σ_j as specified above, the second empirical rule is seen to be justified analytically, and therefore it can also be called semiempirical.

The values of σ_{tot} listed in Table IV for the curves marked a have magnitudes in the range 0.27×10^{11} to 5.3×10^{11}/cm^2, and thus are not particularly large. These curves all have the same boundary concentrations, $n_0^{(1)}=4\times10^{10}$/cm^2, $n_0^{(2)}=1\times10^{10}$/cm^2, $n_N^{(1)}=4\times10^{7}$/cm^2, and $n_N^{(2)}=1\times10^{7}$/cm^2. The boundary concentrations for the curves marked b or B are an order of magnitude larger. The corresponding values of σ_{tot} for the uncrossed profile cases lie in the range 13.4×10^{11} to 25.8×10^{11}/cm^2, which are considerably larger than for the curves designated a. On the other hand, the curves marked b or B for the case of crossed profiles have magnitudes for σ_{tot} of 0.57×10^{11} and 6.73×10^{11}, which are not much larger than for some cases of the curves marked a. This provides additional evidence that a profile crossing results in a considerable neutralization of space charge, with the accompanying lessening of space-charge modifications of the growth rate.

Another very interesting feature of Table IV is the fact that the two cases for which V_N is extremely small (0.002 and -0.014 V) have ratios $t_{\text{SC}}/t_{\text{NSC}}$ very close

to 1, corresponding to almost no space-charge modification of the growth rate. This is true even though σ_{tot} is relatively large and the electric fields in the film are found to have values which range in magnitude as large as 10^5 V/cm. (The concentration profiles are of course greatly modified by the space charge.) Furthermore, a comparison with values of t_{SC}/t_{NSC} in the table for calculations in which σ_{tot} is not significantly larger but for which V_N is considerably larger (e.g., consider the cases of V_N being 0.167 and -0.174 V, with corresponding σ_{tot} values of -35.2×10^{11} and 28.7×10^{11}/cm^2) illustrates that the rate in the higher potential cases is considerably affected by space charge. A corresponding comparison can be made for the calculations listed in Table IV for which V_N has the values 0.173, 0.066, 0.002, -0.073, and -0.179 V, with the same result. On this basis, we propose our third empirical rule for space-charge effects: *For a given total space charge in the film, the extent to which the growth rate is modified by the space charge is proportional to the magnitude of the kinetic potential. For example, for the case of zero kinetic potential, the growth rate (in contrast to the concentration profiles) is unmodified by space charge, and is the same as the growth rate predicted from Fick's first law for diffusion as applied to the ionic species in zero electric field.*

Temperature Effects

Most computations were performed utilizing a temperature of 300°K; the dot-dashed curves in Fig. 9 illustrate the essential effects of raising the temperature from 300°K (solid curves) to 600°K, without a change in the other parameters. Note that σ_{tot} increases significantly with increasing temperature, while the normalized value of $J_{NSC}-J_{SC}$ decreases with increasing temperature. Therefore, even though the total space charge increases, the space-charge modification of the growth rate for fixed boundary concentrations is less at higher temperatures. The decreasing effectiveness of space charge on growth rate at elevated temperatures *for fixed boundary concentrations* is in qualitative agreement with the inverse temperature dependence predicted by the perturbation[8,10] and averaging[9] techniques.

An examination of the concentration profiles (not shown) for the 300 and the 600°K computations shows immediately that the larger total space-charge concentration in the 600°K case is due to the fact that the concentration profiles for the two oppositely charged species do not pull together as much at 600°K as they do at 300°K, so that there is less space-charge neutralization at each point in the film. The linear dependence of the equilibrium potentials on temperature leads to an increase in the kinetic potential by a factor of almost 2. The electric fields are significantly larger also at 600°K than at 300°K. The time of growth to 20 monolayers decreases enormously (by a factor of approximately 3.3×10^{-6}) at 600°K relative to 300°K owing to the vastly increased mobilities.

Ohmic Effects for Rate-Limiting Species

The axiomatic basis[24] for the present work is the assumption of particle transport by diffusion currents with fixed boundary concentrations for each diffusing species which are established by the interfacial reactions. The dot-dashed curves in Figs. 4 and 5 illustrate the effect on the concentration profiles in a 50-monolayer film produced by changing the smaller boundary concentration of the rate-limiting species to a value equal to that at the opposite interface, as would be the case in the low-space-charge limit for an "ohmic" species (i.e., a species with no net concentration gradient). It is noted in Figs. 4 and 5 that the profile of the rate-limiting species is modified only near the outer interface, while the profile of the oppositely charged species is hardly changed at all. Thus the space-charge concentration profile (these and subsequent curves are not shown) and the curve for the electric field versus position for each of the two cases are modified significantly only at the outer interface, the modification being quite large in the case of Fig. 4 because the major space-charge species is involved, but almost negligible in the case of Fig. 5 because it is the minor space-charge species which is involved. In the case of Fig. 4, σ_k achieves almost the same value at the outer interface as it has at the metal-oxide interface. The potential versus position in the film is changed somewhat for Fig. 4 but changed negligibly for Fig. 5. The curves for the film-thickness dependence of the total space charge and the electric field at the outer interface are likewise modified somewhat in magnitude but not in shape, while the film-thickness dependence of the electric field at the metal-oxide interface is almost unchanged in both cases. The curves illustrating the film-thickness dependence of $J_{NSC}-J_{SC}$ are unperturbed in shape, the values themselves being modified by less than 5%. The film thickness versus time and the kinetic potential versus time are likewise affected very little.

Therefore it is concluded that the explicit value chosen for the outer boundary concentration of the species which is strongly rate-limiting is not important insofar as it does not appreciably affect the results for the kinetics. (This boundary concentration could even vary arbitrarily with film thickness without affecting the final results.) The physical reason for the unimportance of the value of this particular boundary concentration is the fact that transport of the rate-limiting species is field-controlled and hence it does not depend very strongly on the concentration gradient.

Charge Neutrality at the Interfaces

The tendency toward partial neutralization of the space charge observed in the thicker films at large boundary concentrations raises the question of whether or not the departure from neutralization is due merely to the choice of unequal boundary concentrations for the oppositely charged species. Two calculations were

therefore performed in which the boundary concentrations of the oppositely charged species were chosen to be equal at the interfaces. The resulting curves (not shown) illustrate that charge neutrality is not obtained in this manner; instead, the surface-charge and space-charge fields are of the same order as those for the more general cases. For example, a computation with $n_0^{(2)}$ and $n_N^{(2)}$ chosen to have the same values as $n_0^{(1)}$ and $n_N^{(1)}$, respectively, but otherwise similar to the one given by curve b of Fig. 12, has values of σ_{tot} at $N=20$ in the neighborhood of $13\times10^{11}/cm^2$, with electric fields in the film between 5×10^4 and 3×10^5 V/cm. The concentration profiles and their variation with increasing film thickness are much the same as those illustrated in Fig. 4. The one curve which has a significantly different appearance is that for σ_k versus k/N, since this curve approaches zero at each interface. The rate is considerably retarded by the space charge in the film, in agreement with the qualitative behavior predicted by the three empirical rules.

The results of these computations therefore illustrate that the coupled-currents condition of equal charge-current magnitudes for the oppositely charged diffusing species is the determining factor for the surface-charge and space-charge fields, so that these fields will be created whenever the ionic and electronic conductivities in the film are unequal, as is generally the case. The partial neutralization which occurs for higher boundary concentrations and thicker films is merely a result of the fact that electric fields have been established which are sufficient to equalize the currents, and any further increase in the magnitude of the field would unbalance the currents and therefore cause the coupled-currents condition to be violated. It is of considerable significance that the partial space-charge neutralization which is observed in the present work is a direct result of the macroscopic electric field in the film as deduced from Poisson's equation, and is not a result of strong Coulomb (or chemical) forces between individual oppositely charged defects.[6]

Dependence on Z Value

All calculations described thus far correspond to the choice $Z^{(1)}=1$ and $Z^{(2)}=-1$. As shown in the previous section on the homogeneous-field approximation, the choice of equal magnitudes for the Z values yields a kinetic potential in the absence of space charge which is independent of thickness. A series of computations have been performed with parameters chosen to have the values utilized for curves a and B in the lower part of Fig. 7 but with $Z^{(1)}$ chosen to have values of 2 and 4. (Curve B in Fig. 7 corresponds to curve B in Fig. 2; thus species 1 is both the rate-limiting species and the major space-charge species in the present example.) The most immediate consequence of increasing the value of $Z^{(1)}$ is a noticeable increase in the space-charge density σ_k; at the metal-oxide interface the full increase is noted, but the increase is less inside the film due to the pulling together of the concentration profiles with the resulting partial neutralization of the space charge. The curves for σ_{tot} versus N have the same shape, but increase in value by approximately 70% with increase in $Z^{(1)}$ from a value of 1 to the value of 2, and increase by approximately 40% with increase in $Z^{(1)}$ from the value 2 to the value 4. The (retarding) effect on growth rate is increased by the additional space charge, in accordance with the three empirical rules for space-charge effects.

Of course, the over-all growth rate increases greatly with the value of $Z^{(1)}$, especially in the nonlinear diffusion region. In the linear diffusion region, the mobility increases linearly with the Z value.

The kinetic potential is perturbed by the additional space-charge at higher values of $Z^{(1)}$, as in Fig. 12. In addition, V_N in the homogeneous-field limit, as well as in the case for the inhomogeneous field, has a sharp decrease in value with decreasing thickness in the region of the first several monolayers; this is due to the fact that the unequal magnitudes of the Z values cause V_N to be perturbed by nonlinear effects, as mentioned in the section on the homogeneous-field limit. The film thickness versus time curves are not noticeably perturbed by this behavior of the potential. These early-stage variations of V_N with thickness for unequal Z values and the effect on the kinetics have been studied in greater detail by Mosley.[28]

To summarize, increased Z values cause (a) a perturbation in the early-stage potential and kinetics in the homogeneous-field limit and in the inhomogeneous-field case because of nonlinear diffusion effects, (b) increased transport rates in both the nonlinear and linear diffusion regions due to the larger force per particle exerted by a given electric field, and (c) increased space charge in the film with the accompanying space-charge modifications of growth rate. The second of these effects is important whenever the increase in Z value occurs for the rate-limiting species, and the third of these is important whenever the increase in Z value occurs for the major space-charge species.

Dependence on Lattice Parameter

The lattice parameter a is clearly an important factor in growth rate, since the nonlinear effects of a given electric field on diffusion increase enormously with the value of a, and the mobilities depend on a^2 in the region in which the currents vary linearly with electric field. Computations were carried out corresponding to those of Fig. 12 but with the a value increased by factors of 5 and 10. These calculations indicated a direct scaling to thicker films and lower defect densities.

Let a be replaced by λa and the interfacial areal defect densities $n_0^{(1)}$, $n_0^{(2)}$, $n_N^{(1)}$, and $n_N^{(2)}$ be replaced by the corresponding densities $n_0^{(1)}/\lambda$, $n_0^{(2)}/\lambda$, $n_N^{(1)}/\lambda$, and $n_N^{(2)}/\lambda$, where λ is an arbitrary dimensionless parameter. (For the following discussion, consider $\lambda>1$.) The solution of this new scaled problem yields the result

that throughout the film the areal defect densities, the space-charge areal densities, and the electric fields are decreased from the ones for the unscaled case precisely by the factor $1/\lambda$. [The scaling of areal defect densities by $1/\lambda$ is actually equivalent to a reduction of bulk concentrations by $1/\lambda^2$, since in general $C(x)=n/2a$.] The total film thickness is increased by the factor λ, while all potentials remain the same. The time to transport a given number of particles is increased by the factor λ. Considering the fact that the number of particles per monolayer should decrease as $1/\lambda^2$, the time to reach a given monolayer number would actually be decreased by the factor $1/\lambda$.

Due to exact superposition of the scaled and unscaled defect profiles, the extent to which the profiles pull together to yield a partial charge neutralization can be considered to be exactly the same for the scaled and the unscaled cases, despite the fact that the charge densities are significantly different in the two cases. It is therefore seen that the pulling together of the profiles is an effect primarily due to the electrostatic potential, instead of the charge densities *per se*.

Transport Currents Directed from Oxide-Oxygen Interface to Metal-Oxide Interface

Since all computations have been for the negative-gradient case, such as for the diffusion of cations and electrons from the metal-oxide to the oxide-oxygen interface, the question arises as to whether the results have any significance for the positive-gradient case, as for example, the diffusion of cation vacancies and positive holes from the oxide-oxygen interface to the metal-oxide interface. The results for the previously presented negative-gradient case can be transformed directly to the corresponding positive-gradient case by interchanging the boundary concentrations at the two interfaces for each given species and replacing each value of $Z^{(s)}$ by the corresponding value $-Z^{(s)}$. Thus the case of positive cations diffusing outward under a gradient produced by the fixed areal densities $n_0^{(1)}=4\times10^{10}$ and $n_N^{(1)}=4\times10^7/\text{cm}^2$ transforms to the case of negative cation vacancies diffusing inward under a gradient produced by the fixed areal densities $n_N^{(1)}=4\times10^{10}$ and $n_0^{(1)}=4\times10^7/\text{cm}^2$. The ionic and electronic mobilities are considered to be unchanged. In continuum notation, the various quantities for this positive-concentration-gradient case can be obtained very simply from the corresponding quantities calculated for the negative-concentration-gradient case by the transformations $C(x)\rightarrow C(L-x)$, $\rho(x)\rightarrow-\rho(L-x)$, $E(x)\rightarrow-E(L-x)$, and $\{V(x)-V(0)\}\rightarrow-\{V(L-x)-V(L)\}$. Note that the transformed potential is renormalized so that it remains zero at the metal-oxide interface. The growth rate is of course unchanged.

Correlation with Experimental Data

Experimental determination of the causes for the manifestation of a given type of oxidation kinetics by a system has not advanced to the point where definite correlations between theory and experiment can be made unambiguously. Departures from the parabolic growth law are commonly observed[34]; in certain cases (e.g., copper,[35] iron,[36,37] and sodium[38]) these are frequently in the retarding direction, while in others (notably aluminum[39] and hafnium[40]) these are at higher temperatures in the enhancing direction. Thus there is qualitative agreement between theory and experiment.

The complexity of the space-charge equations precludes any extensive quantitative fitting of experimental data utilizing the exact numerical computations; however, the approximate equations of previous analytical developments indicate satisfactory agreement with experimental data, as illustrated in Refs. 9 and 10. The present numerical computations provide support for the predictions of these approximate analytical developments, and in this sense quantitative agreement between theory and experiment can be said to be satisfactory.

V. CONCLUSIONS

Space charge generally modifies growth kinetics from the functional form appropriate for a homogeneous field, as summarized by the following semi-empirical rules:

(1) Space charge retards the growth rate whenever the sign of the rate-limiting species is the same as the sign of the total space charge in the film; space charge enhances the growth rate whenever the sign of the rate-limiting species is opposite to the sign of the total space charge in the film.

(2) For a given kinetic potential, the extent to which the growth rate is modified by space charge is qualitatively proportional to the total space charge in the film, which in turn depends on the boundary concentrations and the character of the concentration profiles.

(3) For a given total space charge in the film, the extent to which the growth rate is modified by the space charge is proportional to the magnitude of the kinetic potential. For example, for the case of zero kinetic potential, the growth rate (in contrast to the concentration profiles) is unmodified by space charge, and is the same as the growth rate predicted from Fick's first law for diffusion as applied to the ionic species in zero electric field.

---

[34] O. Kubaschewski and B. E. Hopkins, *Oxidation of Metals and Alloys* (Butterworths Scientific Publications, Ltd., London, 1953).

[35] T. N. Rhodin, J. Am. Chem. Soc. **73**, 3143 (1951).

[36] H. T. Yolken and J. Kruger, J. Electrochem. Soc. **114**, 796 (1967).

[37] M. Wym. Roberts, Trans. Faraday Soc. **57**, 99 (1961).

[38] J. V. Cathcart, L. L. Hall, and G. P. Smith, Acta Met. **5**, 245 (1957).

[39] E. A. Gulbransen and W. S. Wysong, J. Phys. Chem. **51**, 1087 (1947).

[40] W. W. Smeltzer and M. T. Simnad, Acta Met. **5**, 328 (1957).

APPENDIX: RELATIONSHIP BETWEEN ACTUAL CHARGE AND EFFECTIVE CHARGE PER PARTICLE OF A SPECIES DIFFUSING IN A POLARIZABLE AND PARTIALLY COVALENT MEDIUM

In the limit of equilibrium, the relationship between the areal densities of charged particles in adjacent potential minima is given by the Boltzmann factor, so that

$$n_k = n_{k-1} \exp(-\Delta U_{k-1}/k_B T), \quad \text{(A1)}$$

where ΔU_{k-1} is the difference in potential energy between the two positions. The energy ΔU_{k-1} is simply the product of the *actual* charge per particle of the diffusing species and the electrostatic potential difference ΔV_{k-1} between the two positions,

$$\Delta U_k = q\Delta V_{k-1} = -2qaE_k, \quad \text{(A2)}$$

where Eq. (2.6) has been utilized.

In addition, at equilibrium the particle current J_k is zero, in which case Eq. (2.12) [i.e., Eq. (2.5) of Ref. 17] yields

$$n_k = n_{k-1} \exp(2ZeE_k a/k_B T). \quad \text{(A3)}$$

Comparison of (A3) with (A1) shows that

$$\Delta U_k = -2ZeE_k a. \quad \text{(A4)}$$

Comparing (A2) with (A4) yields the result $Ze = q$.

PHYSICAL REVIEW VOLUME 175, NUMBER 3 15 NOVEMBER 1968

Electron-Spin Susceptibilities of the Liquid Binary Alkali Metal Alloys*

J. A. KAECK†
Laboratory of Atomic and Solid State Physics, Cornell University, Ithaca, New York 14850
(Received 22 April 1968)

We report measurements of the Knight shifts of the liquid binary alkali metal alloys over the entire range of concentration of constituents for the alloys Na-Cs, K-Rb, K-Cs, and Rb-Cs. We interpret all existing measurements of the Knight shift in the binary alloys of Na, K, Rb, and Cs to give the electron-spin susceptibility χ_e of those pure alkalis not previously measured. Our interpretation uses the assumption that $\langle|\psi(0)|^2\rangle_{E_F}$ for a particular constituent of a particular alloy remains constant, equal to that for the pure metal, over the entire concentration range in that alloy. In previous work on the alkali alloys, the changes in the Knight shift in dilute alloys were attributed solely to changes in $\langle|\psi|^2\rangle_{E_F}$ due to scattering by impurity atoms, whereas we attribute the changes primarily to changes in χ_e and the atomic volume. New results for pure metals, in cgs volume units, are $\chi_e = (0.84\pm0.08)\times10^{-6}$ for potassium and $\chi_e = (0.80\pm0.08)\times10^{-6}$ for both rubidium and cesium. Our values are based upon the measured value $\chi_e = 1.13\times10^{-6}$ for sodium as a calibration point. The inferred susceptibilities are consistent with values of the parameter ξ of 0.69 ± 0.07, 0.72 ± 0.07, and 0.79 ± 0.08 for potassium, rubidium, and cesium, respectively, where ξ is the ratio of electron wave function density at the nucleus in the metal to the same quantity in the free atom. We compare the inferred susceptibilities with the calculations of Silverstein. We also make comparisons via the measured total susceptibilities for the alkalis with some existing calculations of the diamagnetic and ionic susceptibilities for these metals.

I. INTRODUCTION

A QUANTITY of considerable interest in the modern theory of metals is the conduction-electron-spin susceptibility χ_e of the simple metals. There exist in the literature direct measurements of values of χ_e of Li and Na.[1–3] The measurement technique used to obtain the value of χ_e is that of Schumacher and Slichter.[1] The experiment consists of the comparison of the integrated conduction-electron spin-resonance (CESR) absorption to the integrated nuclear magnetic resonance (NMR) absorption at constant frequency. The technique has not yet been applied to simple metals other than Li or Na because of unfavorably large CESR linewidths of the other metals.[4,5]

We present a technique by which we obtain values of χ_e for K, Rb, and Cs by means of an indirect measurement of χ_e in the liquid binary alkali alloys. Our technique uses the Knight shifts[6] of the liquid binary alkali alloys of Na, K, Rb, and Cs. We use the results

* Work supported in part by the U.S. Army Research Office (Durham) under Contract No. DA-31-124-ARO-D-407, Technical Report No. 9, and by the Advanced Research Projects Agency through the Materials Science Center at Cornell University, Report No. 914.

† Present address: Department of Physics, Ohio State University, Columbus, Ohio.

[1] R. T. Schumacher and C. P. Slichter, Phys. Rev. **101**, 58 (1956).

[2] R. T. Schumacher and W. E. Vehse, J. Phys. Chem. Solids **24**, 297 (1963).

[3] R. Hecht, Phys. Rev. **132**, 966 (1963).

[4] G. Feher and A. F. Kip, Phys. Rev. **98**, 337 (1955).

[5] Sheldon Schultz and M. R. Shanabarger, Phys. Rev. Letters **16**, 178 (1966); W. M. Walsh, Jr., L. W. Rupp, Jr., and P. H. Schmidt, *ibid.* **16**, 181 (1966).

[6] W. D. Knight, Phys. Rev. **76**, 1259 (1949).